Development of transmembrane potential in concentric spherical, confocal spheroidal, and bispherical vesicles subjected to nanosecond-pulse electric field

Shoubhanik Nath, Kumari Priti Sinha,* and Rochish M. Thaokar†
Department of Chemical Engineering, IIT Bombay, Mumbai 400076, India

(Received 23 March 2020; accepted 11 May 2020; published 8 June 2020)

Electroporation of concentric compound spherical and confocal spheroidal as well as eccentric compound spherical vesicles, considered to be good models for corresponding nucleate cells, are investigated with an emphasis on their response to nanosecond pulse electric field (nsPEF). Analytical models are developed for the estimation of the transmembrane potential (TMP) across the bilayers of the inner and the outer vesicles and finite-element simulations are also carried out for the eccentric case. Our calculations show that with an increase in the aspect ratio, while the TMP decreases when nsPEF is used, it increases for confocal spheroids when the pulse width is greater than the membrane charging time, leading to fully charged vesicles. Bipolar pulses are shown to effectively control the TMP for a desired time period in the nsPEF regime, and a fast decay of the TMP to zero can be achieved by judicious use of pulse polarity. The external conductivity is found to significantly influence the TMP in nsPEF, unlike millisecond pulses where its effect is insignificant. Additionally the critical electric field required to induce a TMP of 1 V at the inner vesicle is presented for different pulse widths, rise time, as well as membrane capacitance, and the TMP of the outer vesicle is found to be within limits of reversible poration. It is found that the maximum TMP has a roughly linear dependence on the outer aspect ratio of the vesicle. We also introduce a new method to obtain the particular solution to the Laplace equation for bispherical system, and it is validated with finite-element simulations. Our study on nsPEF electroporation of bispherical vesicles shows that the north pole TMP is typically greater than the south pole, thereby suggesting the typical pathway a charged species might take inside an eccentric nucleate cell under electroporation.

DOI: 10.1103/PhysRevE.101.062407

I. INTRODUCTION

The selectively permeable cell and nuclear membranes in nucleate cells resist the movement of polar molecules and ions, such as drug molecules, across them. Electroporation has emerged as a promising method for cancer chemotherapy, wherein pores formed in a bilayer (cell) membrane, due to application of strong electric pulses, are known to facilitate the uptake of anticancer drugs directly into the cell [1]. A typical pore formation mechanism in a bilayer membrane is a balance of the pore energy enhancing line tension term, dependent on the perimeter of a cylindrical pore, and the pore energy diminishing surface tension that is dependent on the cross-section area of the pore. The barrier to poration is typically of the order of several hundreds of k_BT where k_B is Boltzmann constant and T is temperature. This barrier is significantly reduced by applying an electric field across the cell or a vesicle. The application of electric field builds a transmembrane potential across the vesicle (cell) membrane, and leads to an area- (cross-sectional area of the pore) dependent reduction in the energy of the pore that is proportional to the difference in the permittivity of water and the hydrocarbon tails, and varies as square of the transmembrane potential (TMP) [2].

Application of electric field causes stresses on the membranes and forces the lipid membranes to undergo structural changes, thereby forming pores on the cell surface, through which material can pass through. Although traditional methods of cell electroporation only aim to porate the cell membrane, it is worth mentioning that nanosecond pulsed electric fields (nsPEF) have been recently suggested for calcium release, enhanced gene expression, [3], human cancer cell death [4], and electroporation wherein intense, ultrashort pulses are provided to porate both the cell and the organelle membranes simultaneously [5,6]. This makes it possible to introduce drugs or other genetic materials into organelles or the cell nucleus. When an electric field is applied, TMP develops across the vesicle (cell) membranes and at values of TMP usually of the order of 1V [7], pores are seen to form on the surface of the membrane. Denzi *et al.* [8] suggest that nsPEF can be used to porate the lysosomal and cell membranes simultaneously for release and uptake of anticancer drugs. Electroporation using nsPEF has to be done carefully as application of a very high field for longer durations can result in rupture of the cell membrane [1] and consequent cell death. A theoretical model is, therefore, needed to study the temporal development of TMP due to ac or dc fields. However, the task is further complicated by nonspherical shapes of the cells. Moreover, even spherical cells can undergo deformation, typically prolate spheroidal [9,10] under the application of electric field.

Tumor cell cultures can be spheroidal in shape [11], as are tumor cells [12,13]. Bacterial cells such as yeast and *Pseudomonas* sp. are prolate spheroids [14], while carcinomic cells can also be approximated to be spheroidal in nature. Thus, modeling a nucleate cell as a confocal compound

*Present address: Univ. Grenoble Alpes, CNRS, LIPhy, 38000 Grenoble, France.
†rochish@che.iitb.ac.in

prolate spheroidal system is a reasonable approximation in many cases. Simple models, where the cell has been modelled as a spheroidal vesicle (prolate or oblate) while neglecting the effect of nucleus and other organelles, to study cell electroporation [14] and cell deformation [15] and cylindrical cell shapes representing nerve cells [16] have been suggested in literature. Numerical schemes, such as finite-difference methods to solve for the TMP in spheroidal cells [17] can also be used to overcome the geometric constraints of an analytical model. Yet another way to model the cell is to develop an equivalent electric circuit for the cell, considering the cell membranes as capacitors and solving for the equations to yield a time varying TMP. The method has been adapted for different cell shapes and configurations such as concentric spherical shells, modeling both the outer cell membrane and an inner oragnelle [18]. Theoretical treatments of solving the governing equations in Laplace domain for a transfer function–based model to analyze the time-varying nature of the TMP and also a more general transfer function–based approach for concentric spherical cells have been fairly successful [19–22]. A relatively new model for nucleate, nonspherical cells is the confocal spheroidal model [23] where the development of TMP for arbitrary orientation due to subnanosecond pulses and steps, in the presence of electroporation, was numerically simulated to investigate the TMP distribution with polar angle after pore formation by simultaneous solution of the Laplace and Smoluchowski equations, but the explicit dependence of the electrical, geometric, and input parameters were not shown, nor was the geometric constraints discussed.

It should be noted that concentric spherical or confocal spheroidal models are approximations to the cell and seldom are the cell and the target organelle or nucleus concentric or confocal with respect to the cell. In this work, we also put forward a theoretical model using bispherical coordinate system to study the development of TMP on cells with eccentric organelles (henceforth called eccentric cells) and the deviation that eccentricity causes to the TMP distribution in the inner and outer vesicles. To the knowledge of the authors, to date, there has been no body of work in literature pertaining to theoretical model of eccentric cells. Bispherical systems are well established and are frequently used in standard two-sphere problems in electrostatics [24,25]. Potential equations in bispherical systems are almost always solved using a perturbation-based technique due to the inconsistent system of equations that arise inevitably in such coordinate systems and thus the solution methodology is often problem specific.

The above discussion leads to the following questions for which we seek answers in the present work. An analytical method for estimation of TMP in confocal spheroidal systems is suggested, and comparison is made with numerical calculations. Further, an analytical model for the potential distribution and temporal evolution of TMP in an eccentric cell is provided and a general method to provide particular solution for problems in this coordinate system is suggested. Answers are then sought to the following questions: (i) What is the variation of TMP of the inner and outer vesicles in a confocal spheroidal system with aspect ratio. (ii) What is the variation of the critical electric field required to generate a TMP of 1 V in the inner vesicle as function of aspect ratio, pulse width, rise times, membrane capacitance and outer medium conductivity.

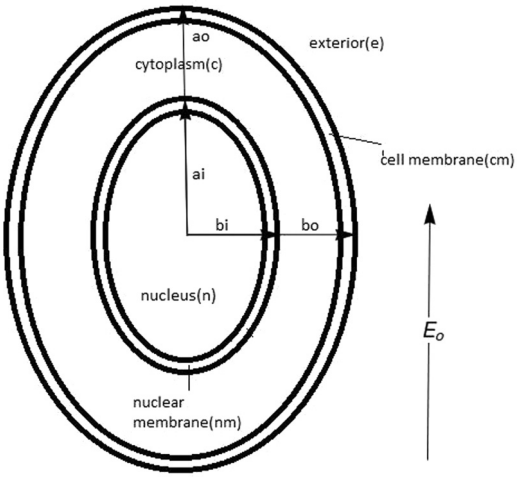

FIG. 1. A schematic of the confocal spheroidal system geometry, highlighting the important lengths and domains. The actual shapes of the inner and outer vesicles are different.

(iii) Can bipolar pulses be used to control the TMP in nsPEF systems (iv). In a bispherical system of eccentric vesicles, is the poration likely to occur at the north pole or the south pole of the inner and outer vesicle?

II. PROLATE SPHEROIDAL MODEL

A. Prolate spheroidal coordinates

Prolate spheroidal coordinate is used to model the cell, with the nucleus also as a spheroid, having the same focus as that of the outer cell. In the present model, ψ denotes the azimuthal angle, ξ characterizes the family of confocal ellipsoids, and η characterizes the family of hyperboloids. The semimajor and semiminor axis lengths are a and b, respectively (Fig. 1), $\lambda(=\frac{a}{b})$ is the aspect ratio, and $c(=\sqrt{a^2-b^2})$ is the semifocal length. In prolate spheroidal coordinates, the polar diameter is more than the equatorial diameter ($a > b$) and the opposite is true ($b > a$) in oblate spheroids. The relations to Cartesian coordinates are $x = c\,\sinh u\,\sin\nu\,\cos\psi$, $y = c\,\sinh u\,\sin\nu\,\sin\psi$, $z = c\,\cosh u\,\cos\nu$. Further convenient substitutions, $\xi = \cosh u$, $\eta = \cos\nu$ are then made to obtain equations in ξ and η. The semifocal length in prolate spheroids and its relation to the variable ξ is given by [26]

$$\xi = \frac{a}{c}, \tag{1}$$

and the domains as $1 \leqslant \xi < \infty$, $-1 \leqslant \eta \leqslant 1$, and $0 \leqslant \psi \leqslant 2\pi$. The Laplacian in prolate-spheroidal coordinates is given by [27]

$$\nabla^2 = \frac{1}{c^2}\left\{\frac{1}{\xi^2-\eta^2}\frac{\partial}{\partial\xi}\left[(\xi^2-1)\frac{\partial}{\partial\xi}\right] + \frac{1}{\xi^2-\eta^2}\frac{\partial}{\partial\eta}\left[(1-\eta^2)\frac{\partial}{\partial\eta}\right], + \frac{1}{(\xi^2-1)(1-\eta^2)}\frac{\partial^2}{\partial\psi^2}\right\}, \tag{2}$$

and the relations between prolate-spheroidal unit vectors and Cartesian unit vectors are as follows [28]:

$$\hat{\xi} = \xi\frac{\sqrt{1-\eta^2}}{\sqrt{\xi^2-\eta^2}}\cos\psi\hat{i} + \xi\frac{\sqrt{1-\eta^2}}{\sqrt{\xi^2-\eta^2}}\sin\psi\hat{j} + \eta\frac{\sqrt{\xi^2-1}}{\sqrt{\xi^2-\eta^2}}\hat{k}, \tag{3}$$

$$\hat{\eta} = -\eta\frac{\sqrt{\xi^2-1}}{\sqrt{\xi^2-\eta^2}}\cos\psi\hat{i} - \eta\frac{\sqrt{\xi^2-1}}{\sqrt{\xi^2-\eta^2}}\sin\psi\hat{j} + \xi\frac{\sqrt{1-\eta^2}}{\sqrt{\xi^2-\eta^2}}\hat{k}, \tag{4}$$

$$\hat{\psi} = -\sin\psi\hat{i} + \cos\psi\hat{j}. \tag{5}$$

B. System geometry

The confocal spheroidal model for a vesicle is a realistic model for many cell types as it takes into account the asphericity of the cell and also models the effect of the nucleus. The model figure is shown in Fig. 1 with the abbreviations used mentioned in brackets. The geometry of the system has to be defined properly for confocal spheroids and it should also be noted that there is a lower bound for the inner vesicle, determined by the size of the outer vesicle. Mostly, the electrical and geometrical parameter values used by Kotnik and Miklavčič [19] in their model for concentric spherical shells have been used. The variable ξ characterizing the ellipses can be related to the aspect ratio as

$$\xi_{co} = \frac{\lambda_o}{\sqrt{\lambda_o^2-1}}, \tag{6}$$

$$\xi_{no} = \frac{\lambda_i}{\sqrt{\lambda_i^2-1}}, \tag{7}$$

where $\lambda_o(=\frac{a_o}{b_o})$ is the aspect ratio of the outer spheroid, $\lambda_i(=\frac{a_i}{b_i})$ is the aspect ratio of the inner spheroid. On equating the volume of the spheroid to that of an equivalent sphere, the following relation is obtained,

$$a_o = R_o(\lambda_o)^{\frac{2}{3}}, \tag{8}$$

$$a_i = R_i(\lambda_i)^{\frac{2}{3}}, \tag{9}$$

where R_o is the radius of the outer sphere, and R_i is the radius of the inner sphere. The outer surface of the plasma membrane is defined by ξ_{ce} and the inner surface is defined by ξ_{ci} while the thickness of the outer membrane is given by d_1 and the inner membrane thickness is d_2. The membrane outer surface is equated to the sphere equivalent surface $\xi_{ce} = \xi_{co}$ and the inner surface is similarly given by $\xi_{ci} = \frac{a_o - d_1}{c}$. Similarly, ξ_{ne} and ξ_{ni} characterize the outer and inner surfaces of the nuclear membrane, respectively. The confocal assumption places a restriction [29] on the values that λ_i can take as the focal length must not exceed the semimajor axis length for the inner spheroid and thus there is a lower bound on the inner aspect ratio, governed by the outer aspect ratio. This restriction results in the following relation between λ_i, λ_o, R_o, and R_i:

$$(\lambda_i)^{\frac{4}{3}}\left(1-\frac{1}{\lambda_i^2}\right) = \frac{R_o^2}{R_i^2}\lambda_o^{\frac{4}{3}}\left(1-\frac{1}{\lambda_o^2}\right). \tag{10}$$

Using this equation, plugging in the values for R_o, R_i, and λ_o, values for λ_i are obtained of which only real, positive values greater than 1 should be accepted.

C. Governing equations

The leaky dielectric model (LDM) is employed, which gives rise to charges on the surface and displacement currents across the membranes. The domains are fully resolved, i.e., the governing equations are applied to each of the domains shown in Fig. 1. It has been tacitly assumed that the vesicles do not undergo any deformation under the action of the electric field and maintain their shape throughout, as shape deformations will affect the TMP. The conductivities of the cytoplasm and the nucleoplasm are assumed to be large enough that no charges can exist in the bulk and any convection currents developed will be small, due to the low Reynolds numbers that accompany the flow and are thus neglected. Although the conductivities in the membranes prior to poration are very small, it can be safely assumed that no charges are present in the bulk as the membrane thickness $d \ll R_o$. Thus, in the absence of any bulk charge, the potential distribution in each of the domains is given by the Laplace equation,

$$\nabla^2\phi_l = 0, \tag{11}$$

where l = n, nm, c, cm, and e according to Fig. 1. The system is subjected to a spatially uniform, time-varying electric field along the z axis, which is the vertical axis of symmetry. The boundary conditions are given below as:

From potential continuity at the interface,

$$\phi_i(\xi_{ni}) = \phi_{\rm nm}(\xi_{ni}), \tag{12}$$

$$\phi_{\rm nm}(\xi_{ne}) = \phi_c(\xi_{ne}), \tag{13}$$

$$\phi_c(\xi_{ci}) = \phi_{\rm cm}(\xi_{ci}), \tag{14}$$

$$\phi_{\rm cm}(\xi_{ce}) = \phi_e(\xi_{ce}), \tag{15}$$

and from normal current continuity at the interface

$$K_n\overline{\nabla}\phi_n\cdot\hat{n}|_{\xi=\xi_{ni}} = K_{\rm nm}\overline{\nabla}\phi_{\rm nm}\cdot\hat{n}|_{\xi=\xi_{ni}}, \tag{16}$$

$$K_{\rm nm}\overline{\nabla}\phi_{\rm nm}\cdot\hat{n}|_{\xi=\xi_{ne}} = K_c\overline{\nabla}\phi_c\cdot\hat{n}|_{\xi=\xi_{ne}}, \tag{17}$$

$$K_c\overline{\nabla}\phi_c\cdot\hat{n}|_{\xi=\xi_{ci}} = K_{\rm cm}\overline{\nabla}\phi_{\rm cm}\cdot\hat{n}|_{\xi=\xi_{ci}}, \tag{18}$$

$$K_{\rm cm}\overline{\nabla}\phi_{\rm cm}\cdot\hat{n}|_{\xi=\xi_{ce}} = K_e\overline{\nabla}\phi_e\cdot\hat{n}|_{\xi=\xi_{ce}}, \tag{19}$$

where $\hat{n}$, the unit normal vector from the surface of the spheroids, is nothing but $\hat{\xi}$, whose expression is given by Eq. (3). In the current continuity equations, the K values are the complex conductivities, given by $K = \sigma + \frac{\partial}{\epsilon\partial t}$ [30]. For ac fields, it becomes $K_{\rm ac} = \sigma + i\,\omega\,\epsilon$, with ω as the input field frequency. Similarly, for dc fields, using the Laplace transform on the boundary conditions Eq. (19), the complex conductivities reduce to $K_{\rm dc} = \sigma + \epsilon\, s$, with s as the Laplace domain variable.

TABLE I. Geometric parameter values in SI units.

Parameters	Meaning	Values
R_o	Equivalent outer radius of cell	10×10^{-6}
$d_1(d_2)$	Thickness of the vesicle(nuclear) membrane	5×10^{-9}
R_i	Equivalent outer radius of nucleus(organelle)	3×10^{-6}

TABLE II. Electrical parameter values in SI units.

Parameter	Meaning	Values
σ_n	Conductivity of the nucleoplasm	0.3
ϵ_n	Permittivity of the nucleoplasm	6.4×10^{-10}
$\sigma_{\rm nm}$	Conductivity of the nuclear membrane	3×10^{-7}
$\epsilon_{\rm nm}$	Permittivity of the nuclear membrane	4.4×10^{-11}
σ_c	Conductivity of the cytoplasm	0.3
ϵ_c	Permittivity of the cytoplasm	6.4×10^{-11}
$\sigma_{\rm cm}$	Conductivity of the plasma membrane	3×10^{-7}
$\epsilon_{\rm cm}$	Permittivity of the plasma membrane	4.4×10^{-11}
σ_e	Conductivity of the outer medium	1.2
ϵ_e	Permittivity of the outer medium	6.4×10^{-10}

D. Solution of governing equations in prolate spheroidal coordinates and general response methodology

Using the form for the Laplace operator given by Eq. (2), variable separation is applied to arrive at the well-known Euler's equations. The solutions to Euler's equations are given by spherical harmonics [31] with the eigenfunctions as Legendre functions of first and second kind. Thus, the electric potential is given by

$$\phi_l = \sum_{k=0}^{\infty} [C_{l1} P_k(\xi) + C_{l2} Q_k(\xi)][C_{l3} P_k(\eta) + C_{l4} Q_k(\eta)], \tag{20}$$

where ϕ_l is finite and therefore $C_{l4} = 0$ as Q_k diverges at $\eta = \pm 1$. Now, as $\xi \to \infty$, the electric field should be equal to the externally applied electric field, i.e., $\frac{\partial \phi}{\partial \xi} = -E_o(t)\eta$ [31], giving the value of k to be 1 and $C_{e1} = -E_o(t)c$. Inside the nucleus, ξ can take the value of 1 and hence $C_{n2} = 0$ for the solution to be convergent. Using Eqs. (12) to (19), all the coefficients are evaluated to obtain the complete solution for all the domains. It is to be noted that $P_1(\xi) = \xi$ and $Q_1(\xi) = \frac{\xi}{2} \ln(\frac{\xi+1}{\xi-1}) - 1$. The potential comes out to be linear in η which is equivalent to the polar angle. The TMP across any two surfaces (say, a and b) is written as:

$$V_m = [\phi_a(\xi_a) - \phi_b(\xi_b)]/(E_o \eta), \tag{21}$$

where ξ_a and ξ_b denote the values of the variable defining surface geometry at the two surfaces a and b. The TMP expression is divided by $E_o\eta$ to make the resulting expression independent of η and to obtain a transfer function for the TMP response, as the input electric field is time dependent. For ac inputs, the constants, and hence the TMP, are obtained as a function of the frequency ω. For dc inputs, the constants are functions of the complex Laplace variable. Following the procedure outlined in Ref. [21], the system is subjected to different inputs and inverse Laplace transform is used to get the output response in the time domain,

$$\Delta\phi_m(t) = \mathcal{L}^{-1}[V_m(s)E(s)], \tag{22}$$

where $E(s)$ is the input electric field in Laplace domain. The geometric and electric parameters from the paper by Kotnik and Miklavčič [19] are used and are given in Tables I and II, respectively.

III. MODEL FOR BISPHERICAL SYSTEM

Since real biological cells are seldom concentric in nature, it is necessary to study the deviation of the TMP due to eccentricity and in this section, the bispherical model for the biological cell is discussed to gauge said effect. The model figure of the eccentric cell is given below in Fig. 2(a) with the symmetry axis taken as the z axis. The two poles of the cell are also labeled and the electric field is assumed to be acting from the south (near) to the north (far) pole. It is to be noted that for cells, there are membranes enclosing the cytoplasm and nucleus or organelle, but as the thickness of the membrane is very small compared to the radius of the cells and nuclei, they are not shown here and are assumed to be concentric to their respective structures. Bispherical system is characterized by full spheres, half spheres, and the azimuthal half-plane (not

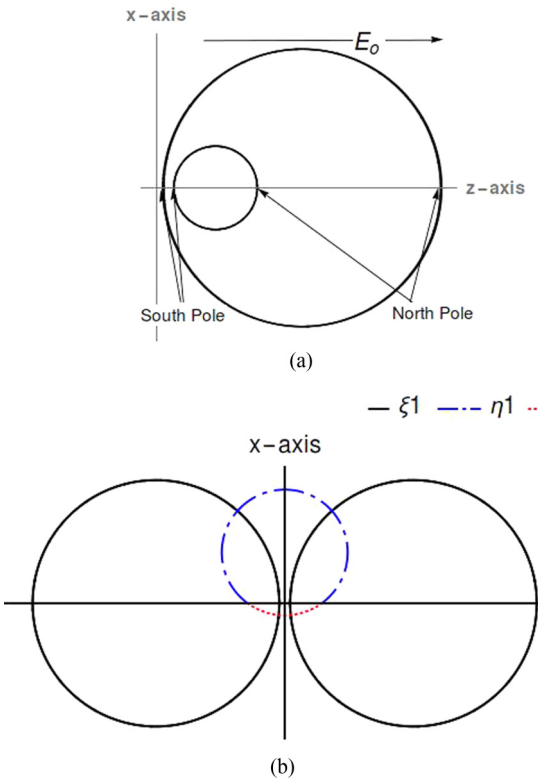

FIG. 2. (a) Diagram of the eccentric cell with the applied electric field along the z axis and the two poles. (b) Representation of the bispherical geometry. The solid black lines represent full spheres, characterized by $\pm\xi_1$. The colored lines represent the half-spheres, characterized by η and two half-spheres, together form one complete sphere. For instance, the dash-dotted blue line represents part of a sphere, characterized by η_1, while the dotted red line represents the remaining part of said sphere, characterized by $\pi + \eta_1$.

shown here). The full spheres in the positive half-plane are characterized by $\xi > 0$, those in the negative half-plane are given by $\xi < 0$ and the half spheres by η as seen in Fig. 2(b).

The variables are related to the Cartesian variables as follows [27]:

$$x = \frac{c\,\sin\eta\,\cos\psi}{\cosh\xi - \cos\eta}; \quad y = \frac{c\,\sin\eta\,\sin\psi}{\cosh\xi - \cos\eta};$$
$$z = \frac{c\,\sinh\xi}{\cosh\xi - \cos\eta}, \tag{23}$$

where ψ denotes the azimuthal angle and c denotes the semifocal length. The externally applied electric field being along the z axis in all the cases, there is azimuthal symmetry in the system and ψ is set to 0. The scale factors are $h_\xi = h_\eta = \frac{c}{\cosh\xi - \cos\eta}$ and $h_\psi = \frac{c\,\sin\eta}{\cosh\xi - \cos\eta}$. The surfaces of constant ξ are given by equation of sphere,

$$x^2 + y^2 + (z - c\,\coth\xi)^2 = \frac{c^2}{\sinh^2\xi}. \tag{24}$$

Therefore, the radii of the whole spheres are $R = c\,\mathrm{csch}\xi$ and their centers are at $(c\,\coth\xi, 0, 0)$. On putting the coordinates $(c, 0, 0)$ in Eq. (24), the resulting value of the left-hand side is less than the right-hand side, indicating that the focus always lies inside the circle. The domains are as $-\infty < \xi < \infty$, $0 \leqslant \eta \leqslant \pi$, and $0 \leqslant \psi \leqslant 2\pi$. The unit vectors for azimuthal symmetry in bispherical system are given by

$$\hat{e_\eta} = \frac{1 - \cos\eta\,\cosh\xi}{\cos\eta - \cosh\xi}\,\hat{i} + \frac{\sin\eta\,\sinh\xi}{\cos\eta - \cosh\xi}\,\hat{k}, \tag{25}$$

$$\hat{e_\xi} = \frac{\sin\eta\,\sinh\xi}{\cos\eta - \cosh\xi}\,\hat{i} + \frac{\cos\eta\,\cosh\xi - 1}{\cos\eta - \cosh\xi}\,\hat{k}. \tag{26}$$

As before, the Laplace equation is solved to get the potential distribution in the various domains, as the bulk charge density is zero.

A. Bispherical model and boundary conditions

Assuming homogeneous media, the outer and inner radii are R_o and R_i, respectively, and the critical geometric parameter, used to define the system is the offset, δ, which is the distance between the centers of the cell and nucleus. The semifocal length can be expressed as a function of the radii and the offset [32]:

$$c = \frac{\sqrt{\delta^4 - 2\delta^2\left(R_o^2 + R_i^2\right) + \left(R_o^2 - R_i^2\right)^2}}{2\delta}. \tag{27}$$

Fixing the radii and the offset gives the semifocal length which is enough information to get the domain boundaries ξ, as

$$\xi = \mathrm{csch}^{-1}\left(\frac{R}{c}\right), \tag{28}$$

where R denotes the radius (which is $R + d$ for the membranes). Table III gives the constants used to characterize the spheres. The Laplace equation [33] in the bispherical coordinate system is $\mathcal{R}$ separable and the separated form is given by

$$\phi(\xi, \eta) = (\cosh\xi - \cos\eta)^{\frac{1}{2}}\,X(\eta)\,Y(\xi), \tag{29}$$

TABLE III. Definition of the surfaces of the system.

Constant	Boundary	Expression
ξ_1	Nucleus-nuclear membrane	$\mathrm{csch}^{-1}(R_i/c)$
ξ_2	Nuclear membrane-cytoplasm	$\mathrm{csch}^{-1}\left(\frac{R_i+d}{c}\right)$
ξ_3	Cytoplasm-cell membrane	$\mathrm{csch}^{-1}(R_o/c)$
ξ_4	Cell membrane-outer medium	$\mathrm{csch}^{-1}\left(\frac{R_o+d}{c}\right)$

with

$$Y(\xi) = \sum_{m=0}^{\infty}\left[A_m e^{(m+\frac{1}{2})\xi} + B_m e^{-(m+\frac{1}{2})\xi}\right], \tag{30}$$

$$X(\eta) = \sum_{m=0}^{\infty}[C_m P_m(\cos\eta) + D_m Q_m(\cos\eta)]. \tag{31}$$

As $\cos\eta$ can take values of 1 and -1, the potential equation reduces to

$$\phi(\xi, \eta) = (\cosh\xi - \cos\eta)^{\frac{1}{2}} \sum_{m=0}^{\infty} \times \left[P_m(\cos\eta)(A_m e^{(m+\frac{1}{2})\xi} + B_m e^{-(m+\frac{1}{2})\xi})\right]. \tag{32}$$

Far away from the cell, $z \to \infty$ and $\phi \to -E_o z$ [34] and the generating function of Legendre polynomials can be used to get z in a form similar to the potential Eq. (32) and the far field condition is juxtaposed into the external potential:

$$z = c\sqrt{2}(\cosh\xi - \cos\eta)^{\frac{1}{2}} \sum_{m=0}^{\infty} P_m(\cos\eta)(2m+1)e^{-(m+\frac{1}{2})\xi}$$

for right half-plane

$$z = -c\sqrt{2}(\cosh\xi - \cos\eta)^{\frac{1}{2}} \sum_{m=0}^{\infty} P_m(\cos\eta)(2m+1)e^{(m+\frac{1}{2})\xi}$$

for left half-plane. (33)

The potential and current boundary conditions, similar to prolate spheroidal system, are applicable here.

B. Solution for bispherical systems

The solution in this coordinate system is far more difficult as the resulting set of equations after putting the appropriate boundary conditions are difference equations which are exact if taken up to infinite terms. The relevant equations, are first, nondimensionalized with characteristic scales R_o for length, $E_o R_o$ for potential, σ_e for conductivity and ϵ_e for permittivity. The characteristic timescale is given by $t_c = \frac{\epsilon_e}{\sigma_e}$ and the inverse of it is the characteristic frequency scale ω_c. The nondimensional potentials are given in Eqs. (B1)–(B5) in Appendix B where a_m to j_m are nondimensional constants which are dependent on m and the south and north poles are characterized by $\eta = \pi$ and $\eta = 0$, respectively. The boundary conditions have been applied at all the four boundaries, and after some substitutions, the difference equations are obtained. For the interface between the nucleus and nuclear membrane, the

equations are

$$\sinh\xi_1\ \alpha_m - \cosh\xi_1\ \beta_m(2m+1) + m\beta_{m-1} + (m+1)\beta_{m+1} = 0, \tag{34}$$

where

$$\alpha_m = K_n\left[b_m e^{2(m+\frac{1}{2})\xi_2} + c_m\right]e^{-(m+\frac{1}{2})\xi_1} - K_{\rm nm}\left[b_m e^{(m+\frac{1}{2})\xi_1} + c_m e^{-(m+\frac{1}{2})\xi_1}\right], \tag{35}$$

$$\beta_m = K_n\left[b_m e^{2(m+\frac{1}{2})\xi_2} + c_m\right]e^{-(m+\frac{1}{2})\xi_1} + K_{\rm nm}\left[b_m e^{(m+\frac{1}{2})\xi_1} - c_m e^{-(m+\frac{1}{2})\xi_1}\right], \tag{36}$$

where K_i's are the complex conductivities, defined before. The system of equations is inconsistent as the number of variables exceed the number of equations and thus, solving for the particular solution is not possible analytically.

C. Solution methodology for bispherical system

The nature of the equations for the constants of the bispherical system is such, that a direct solution is not possible since one has to sum up to infinite number of terms. The methodology adopted in this paper is to truncate the difference equations at some finite value of $m = n$. However, that yields an inconsistent system as the number of variables exceed the number of equations by 4, one for each current continuity equation, leading to a closure problem. One of the exponential eigenfunctions grows and the other one decays and thus, to get a convergent solution, the coefficients associated with the exponentially growing eigenfunctions must decrease faster with increasing value of n. Hence, one can, in theory, drop the $(n+1)$th constants from the system of equations and thus end up with a consistent, approximate system. The value of n to be considered is a matter of trial and error, but one can take high values, subject to the condition that the resultant matrix is not too cumbersome to solve numerically and that the results do not change on increasing the value of n. In most of the literature, a perturbation-based scheme has been employed to overcome the closure problem of the bispherical system. However, in the method presented in this paper, the exact eigenfunctions are retained and it is seen that the solution is convergent for different cases. For the eccentric sphere case, a value of $n = 7$ gives a good result, while for concentric cases, where the offset is small, smaller values of m give an excellent trend. Mathematica software has been used to determine the constants and the potential functions. Adopting the aforementioned methodology, Eq. (34) becomes

$$\begin{aligned}&\sinh\xi_1\alpha_m - \cosh\xi_1\beta_m(2m+1) + m\beta_{m-1} + (m+1)\beta_{m+1} \quad \text{for } 0 \leqslant m \leqslant n-1,\\ &\sinh\xi_1\alpha_n - \cosh\xi_1\beta_n(2n+1) + n\beta_{n-1} = 0 \quad \text{for } m = n,\end{aligned} \tag{37}$$

The other equations are modified accordingly. It should be noted that β_{-1} does not exist, but since its coefficient is zero, the term does not arise in the equations. For $m = n$, there are a total of $4(n+1)$ equations and $4(n+2)$ number of variables, out of which, the four highest-order variables corresponding to $n+1$ are set to zero to close the system of equations, arguing that with increasing value of n, the higher-order harmonics will have lesser and lesser contributions to the stable solution. Care should be taken while solving the system of equations as on increasing values of n, the resultant matrices become ill conditioned. Hence it is not advisable to arbitrarily increase the value of n, for the sake of better accuracy. For simpler cases, as in that of a dielectric sphere in an electric field, small values of n suffice, though one may go up to higher values, like $n = 16$ without jeopardizing the matrix conditioning. In this paper, a value of $n \leqslant 10$ has been followed for the eccentric cell case, unless specified otherwise. The solution methodology is presented in greater detail in the Appendix.

IV. RESULTS FOR CONFOCAL SPHEROIDS

A. Time domain analysis of confocal spheroids

1. Validating the formalism and effect of conductivity

Electric field induced pore formation, or electroporation, is believed to occur when a TMP of around 0.5–1 V is developed across the membrane [35]. In this work, results are presented, assuming that a TMP of 1V can induce electroporation. While classical electroporation techniques use micro- or millisecond pulses to porate just the cell membrane with typical electric field values of 1 to a few 10s of kV/cm [35,36], nsPEF uses a much higher value of electric field, acting for a short time, which increases their ability to penetrate into the cytoplasm causing organelle electroporation, tumor ablation and apoptosis [37]. In electroporation one relevant timescale is the Maxwell-Wagner polarization time, $\tau_{\rm MW} = \frac{\epsilon_i + 2\epsilon_e}{\sigma_i + 2\sigma_e}$ [38], where ϵ_i and σ_i denote the permittivity and conductivity of the cytoplasm or nucleoplasm. The $\tau_{\rm MW}$ for the outer membrane is 0.71 ns for outer conductivity of 1.2 S/m and 6.4 ns for outer conductivity of 10^{-4} S/m. As the membranes act like a spherical capacitor, they have a charging time, $t_{\rm cap} = RC_m(\frac{2\sigma_e+\sigma_i}{2\sigma_e\sigma_i})$ [38], where $C_m = \frac{\epsilon_{nm(cm)}}{d_{1(2)}}$ is the membrane capacitance per unit area. Here the subscript nm and cm represent the nuclear and cell membranes, respectively, and d_1 and d_2 is the nuclear and cell membrane thickness, respectively. The pulse times for nsPEF are typically much smaller than the charging times of the membrane with typical membrane charging time for mammalian cells being of the order of 100 ns [39]. For outer medium conductivities of 1.2 S/m and 10^{-4} S/m the values of $t_{\rm cap}$ are 330 ns and 440 μs, respectively. When the pulse duration is below the membrane charging time, the penetration power of the electric field inside the cell or vesicle increases [6] on account of low membrane impedence.

The confocal spheroidal model can be used as a model system to study the development of TMP in nucleate cells which are deformed or have a nonspherical (spheroidal) geometry. The confocal spheroidal system is identical to the concentric spherical system as the aspect ratio approaches 1 and the results of Kotnik and Miklavčič [19], who had assumed a concentric spherical geometry, have been reproduced during the course of this work by taking a limiting aspect ratio of 1.01, as seen in Fig. 3. Henceforth, aspect ratio 1.01 should be understood to be the concentric spherical vesicle.

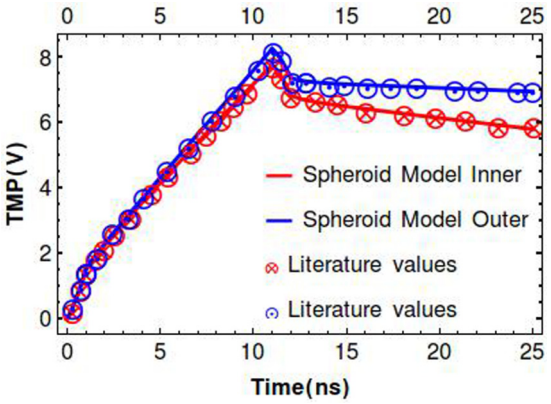

FIG. 3. Variation of TMP with time for confocal spheroid model with inner and outer aspect ratios = 1.01, as limiting case of a sphere, and the concentric spherical model (Kotnik and Miklavčič [19]) for trapezoidal pulse of width 10 ns and rise and fall times of 1 ns. The electrical and geometrical parameters used are from Tables II and I, respectively.

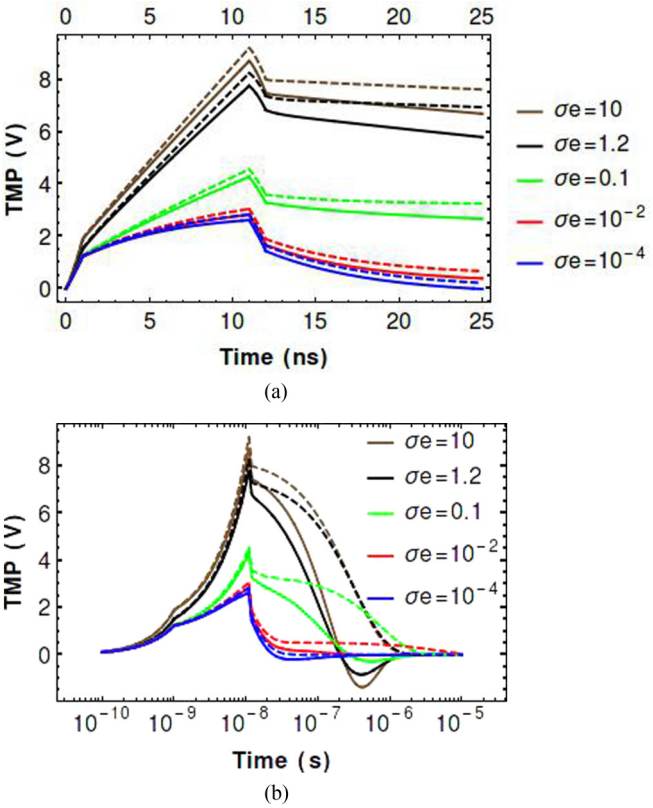

FIG. 4. TMP vs time response curves at different outer medium conductivities, σ_e (in S/m), for the limiting case of confocal spheroids ($\lambda_o = 1.01$, $\lambda_i = 1.01$) under the effect of nsPEF, with input electric field $E_o = 150$ kV/cm are shown here. The solid and dashed lines represent the nuclear (inner) membrane and cell (outer) membrane TMP, respectively. The parameter values have been taken from Tables I and II. (a) Response curves at short times for different conductivities. (b) Response curves at long times for different conductivities.

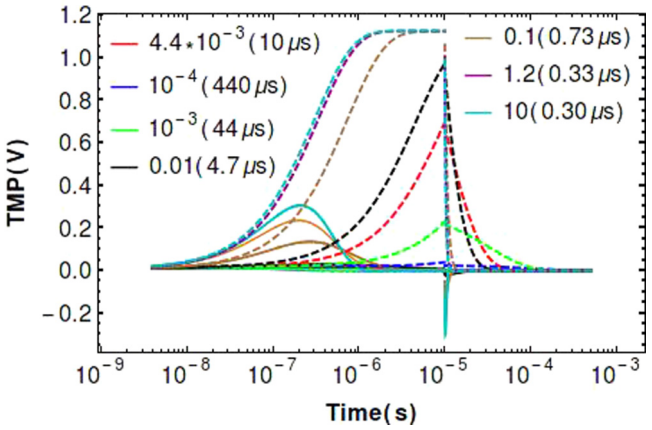

FIG. 5. TMP vs time response curves at different outer medium conductivities (in S/m), for compound spheres ($\lambda_o = 1.01$, $\lambda_i = 1.01$), for 10-μs pulse width, $E_o = 0.75$ kV/cm and parameter values from Tables I and II. The respective capacitive charging times are in brackets. The solid and dashed lines represent the inner membrane TMP and the outer membrane TMP, respectively.

The typical features of the transient development of the TMP in a compound vesicle are shown in the Fig. 3. On application of a nanosecond trapezoidal pulse, the inner and outer TMPs increase with time as both membranes charge over $t < t_{\text{cap}}$. The inner TMP is slightly less than the outer one due to the smaller size of the inner organelle for the same specific membrane capacitances of the inner and the outer membranes. After the pulse is switched off, the TMP shows a sharp decay over the decay time of the pulse, where after the decay happens much slowly over the membrane charging time t_{cap}.

The effect of the outer medium conductivity on the response curves of compound spheres, subjected to a 10-ns pulsed electric field, is shown in Figs. 4 and 5, where the expressions obtained from the confocal spheroidal model has been plotted by taking the limiting case of the aspect ratio ($\lambda_o = 1.01$). The outer medium conductivity predominantly affects the t_{cap} of the outer vesicle. A higher medium conductivity is seen to lead to a faster charging of the outer vesicle, and thereby the TMP at the end of the pulse is higher for larger values of conductivities [Figs. 4(a) and 4(b)]. The decay of the TMP happens over the membrane charging time and a characteristic negative TMP is observed in the inner vesicle when the outer vesicle nears its complete discharge. The nucleus does not experience any electric field when the outer membrane is completely charged. The inner membrane is exposed to a field which has a component, proportional to the derivative of the input pulse and hence, an effective bipolar pulse electric field acts on it, inducing a negative TMP in the inner membrane during the discharge of the outer membrane [6]. To further illustrate the effect of external conductivity, results are presented for a 10-μs trapezoidal pulse input to the vesicle, but now at a much lower electric field of around 0.75 kV/cm.

Clearly, the complete charging of vesicle occurs at high conductivity values, and a TMP of 1.1 V ($3/2E_oR_o$) is reached, independent of the conductivity of the outer medium. This

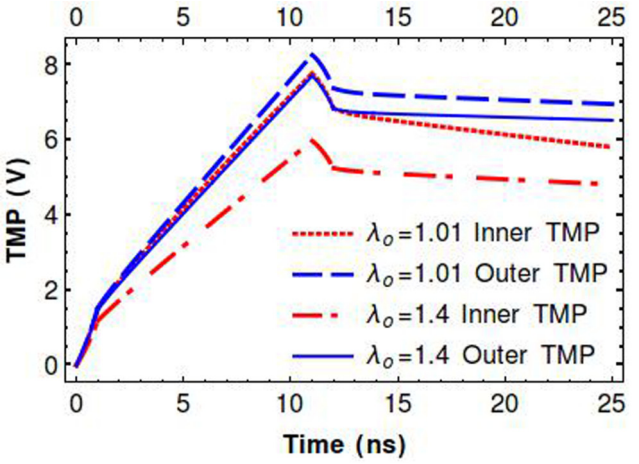

(a)

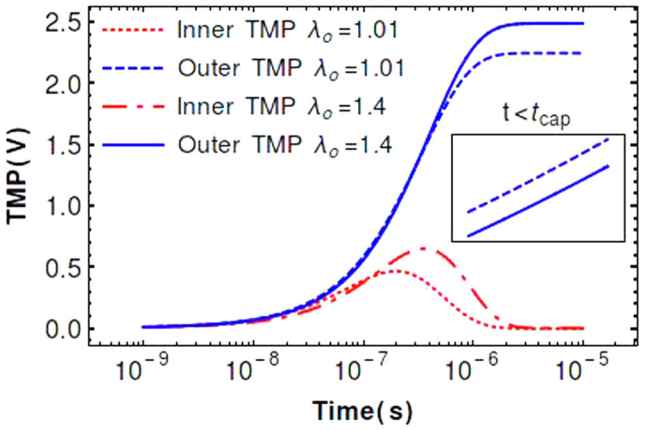

(b)

FIG. 6. TMP vs time response curves under the effect of nsPEF and μsPEF, with $E_o = 150$ kV/cm and parameter values corresponding to Tables I and II. (a) Temporal evolution of TMP for two different aspect ratios for 10-ns pulse width. (b) Temporal evolution of TMP for two different aspect ratios for 100-μs pulse width. The inset of Fig. 6(b) shows the outer TMP evolution for times below the membrane charging time, indicating that at subcharging times, the outer TMP is indeed higher than the inner one. The aspect ratio pairs are ($\lambda_o = 1.01$, $\lambda_i = 1.01$) and ($\lambda_o = 1.4$, $\lambda_i = 5$).

also demonstrates that in pulses (typically millisecond and microsecond pulses) wherein the pulse width is greater than the membrane charging time, one realizes a completely charged membrane with a nondimensional TMP of 1.5, independent of the conductivity. On the other hand, the use of strong electric fields in nsPEF, wherein the pulse width is much shorter than the t_{cap}, one sees a TMP that is sensitively dependent on the conductivity. The sensitivity of the TMP to conductivity in nsPEF is clearly due to the pulse width being smaller than t_{cap}.

2. The effect of aspect ratio

The variation of TMP with the aspect ratio is discussed in this section with reference to Fig. 6. As the aspect ratio increases, i.e., as the vesicle deviates more and more from a spherical shape, the TMP decreases for both the inner and outer vesicles. This is clearly a dynamic effect, wherein for nsPEF, the membrane charging and thereby the TMP is dependent on the membrane charging time. Thus for a confocal spheroidal vesicle, the charging time is higher on account of its higher aspect ratio, as compared to that of a compound spherical vesicle. This leads to smaller TMPs for a confocal spheroid as compared to that of a compound sphere for $t_{pulse} < t_{cap}$. The saturation TMP though for a fully charged compound spheroidal vesicle is greater than that of a compound spherical vesicle. This is on account of the larger effective size of the compound spheroidal vesicle leading to higher saturation TMP (Note the saturation TMP for a spherical vesicle is $3/2E_oR_o$). Thus for milli- and microsecond pulses, (essentially for $t_{pulse} > t_{cap}$) the TMP increases with aspect ratio for a compound spheroidal vesicle. The inset of Fig. 6(b) shows that indeed, at short times, the spherical vesicle has a higher saturation TMP, while at long times, that of the spheroidal vesicle is higher.

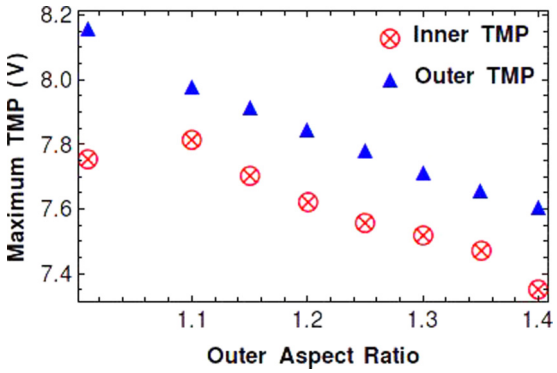

FIG. 7. Effect of outer aspect ratio on the maximum TMP. Parameter values of Table II and I have been used along with an input electric field of $E_o = 150$ kV/cm.

Figure 7 shows the variation of the maximum inner and outer TMP with outer aspect ratio. It is to be noted that the inner and the outer aspect ratios are related [Eq. (10)] and a wide range of values for the inner aspect ratio, corresponding to a fixed outer aspect ratio, can be taken, out of which, values close to the minimum possible have been used in this work. The aspect ratio pairs used are given in Table IV. The figure shows that the outer and inner TMP decrease with an increase in the aspect ratio, indicating that confocal spheroids require a higher voltage to porate their inner and outer membranes as compared to their spherical counterparts.

TABLE IV. Table of aspect ratio pairs for Fig. 7.

Outer aspect ratio	Inner aspect ratio
1.01	1.01
1.1	2.81
1.15	2.9
1.2	3.28
1.25	3.75
1.3	4.28
1.35	4.75
1.4	5.1

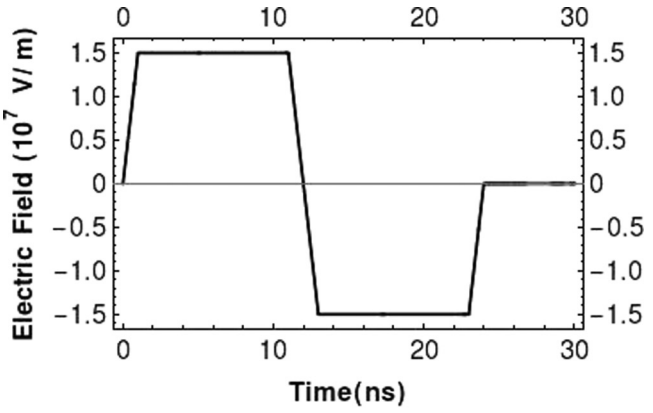

(a)

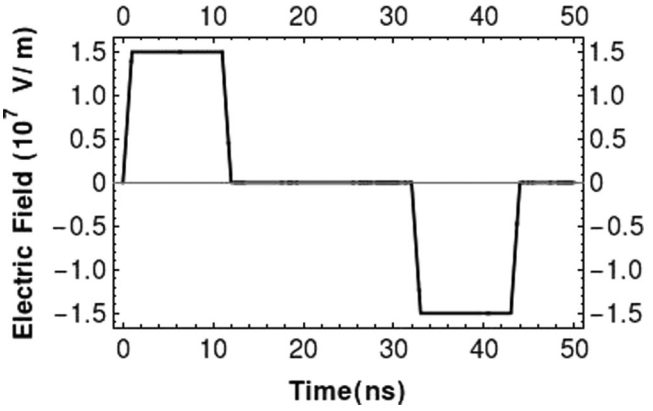

(b)

FIG. 8. The waveforms for bipolar input pulses used in this work. (a) continuous bipolar pulse of amplitude of 150 kV/cm and (b) separated bipolar pulse of same amplitude. The separation time between the two opposite pulses is 20 ns. The pulse width in both the cases is 10 ns, the rise and fall times are 1 ns each.

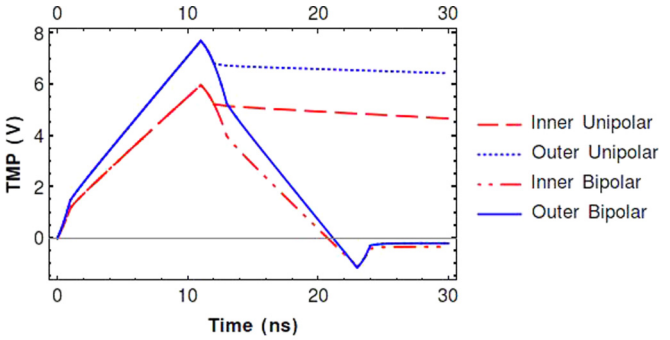

(a)

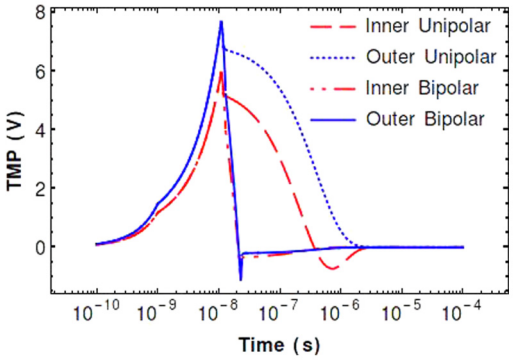

(b)

FIG. 9. TMP vs time response curves to input of Fig. 8(a). (a) Variation of TMP at short times. (b) Variation of TMP at long times. The plots are for spheroidal vesicle ($\lambda_o = 1.4$, $\lambda_i = 5$) using values of Tables I and II.

3. Bipolar pulses

Bipolar pulses are alternating pulses either separated by some finite time difference of no voltage between the pulses or with no such time difference at all and they offer a much better control over the temporal evolution of the TMP. By using bipolar pulses, the time for which the membrane is exposed to high potential values can be controlled and accordingly, excess poration or even lysis of the cell can be easily avoided. This is especially important in nanosecond pulsed electroporation, where strong pulses cannot be applied for long duration. Bipolar pulses are also known to result in symmetrical distribution of pores and better survivability of cells, while achieving the same degree of electroporation as conventional unipolar pulses, although at the expense of higher field intensities [40–42]. Bipolar pulses have also been suspected of achieving greater permeabilization in nonspherical cells or cells with nonhomogeneous membrane [43]. Although nanosecond bipolar pulses have been shown to be less effective compared to their monopolar counterparts [44], bipolar nsPEFs have a canceling effect due to the shifted phase of the second pulse, which merits further investigation into their actions [45]. Figure 8 shows two possible types of bipolar pulses that can be applied to understand the physics of electroporation.

Figures 9 and 10 show that the application of a bipolar pulse leads to immediate reduction in the TMP, and the relaxation over charging time, observed in unipolar pulses, is prevented due to change in the polarity of the electrodes. At the end of the second pulse, the TMP is immediately restored to a very low value. This is more clearly seen when the results are plotted over a longer timescale [Figs. 9(b) and 10(b)]. When the two pulses of the bipolar pulse input are separated with a known time delay, the TMP is nearly held to a constant value at the end of the first pulse, whereafter the TMP can be tuned to zero by application of the second pulse (Fig. 10). This allows a good control over the temporal distribution of the TMP on the inner and the outer vesicle, as can be seen with comparison of an equivalent unipolar pulse, where the membrane experiences significant TMP that decays (relaxes) only over charging times of the order of few microseconds. The faster response observed using a bipolar pulse is clearly due to faster recharging of the membrane due to strong electric fields, but in an opposite direction. The drastic lowering of TMP in the bipolar pulse could also be a cause for the canceling effects of cellular responses seen during the reversing of polarity of pulses [45].

B. Critical electric field

A parametric study is presented in terms of a critical electric field required to induce a threshold TMP of 1V, specif-

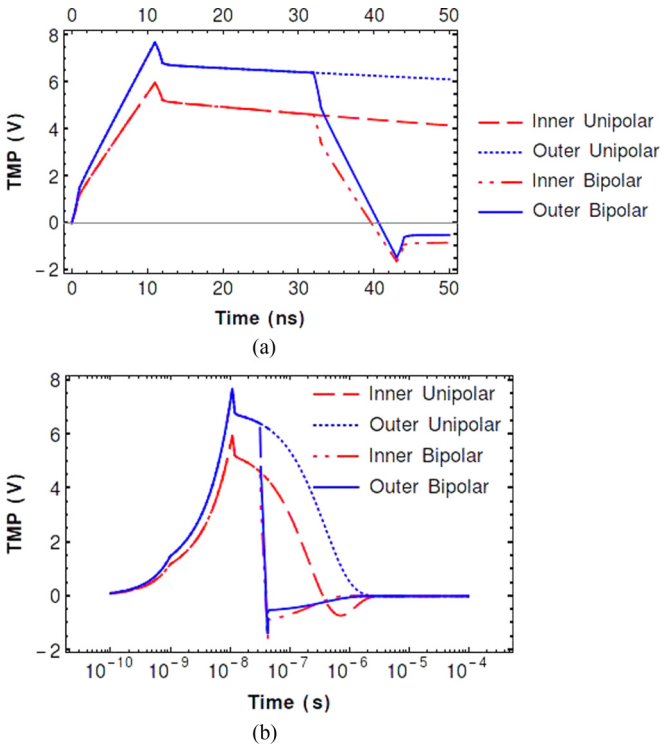

FIG. 10. TMP vs time response curves to separated bipolar pulse input of Fig. 8(b) for compound spheroids ($\lambda_o = 1.4, \lambda_i = 5$) using values of Tables I and II. (a) Variation of TMP at short times. (b) Variation of TMP at long times.

ically on the inner vesicle, since the outer TMP is typically greater than the inner one. It is possible to simultaneously induce the critical voltage of 1 V or more in both the membranes using nsPEF of amplitude 19.4 kV/cm and relaxing to zero over the charge relaxation time, when the aspect ratio is 1.01 (Fig. 11). Since the governing equations are linear, hence the TMP expression also has a linear dependence on the magnitude of the electric field and thus, the trend is independent of the electric field magnitude. A parametric

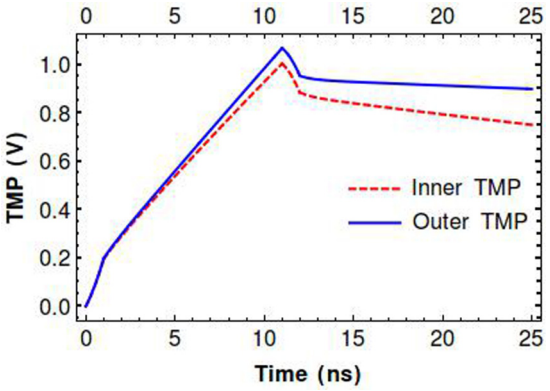

FIG. 11. TMP vs time response at a critical electric field of 19.4 kV/cm for a concentric spherical vesicle. The critical field is selected in such a way as to have a TMP $\approx$ 1 V, while the outer TMP for the selected parameters is always a little higher but not high enough to cause irreversible electroporation. The parameters used are given in Tables I and II.

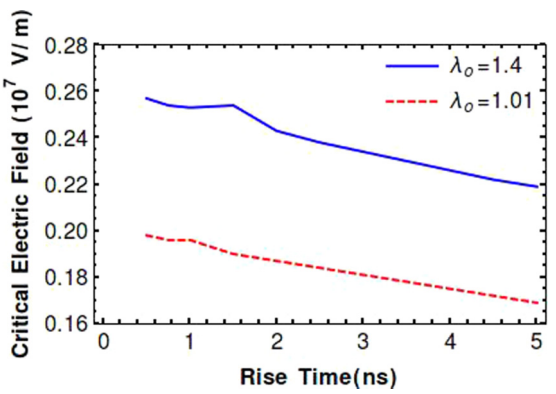

FIG. 12. Effect of rise time on critical electric field. Geometrical and electrical parameters as per Tables II and I, respectively. The aspect ratio pairs are ($\lambda_o = 1.01, \lambda_i = 1.01$) and ($\lambda_o = 1.4, \lambda_i = 5$).

study on variables that can be externally controlled, namely, rise time, pulse width and external conductivity is presented and the goal is to see the effect of the parameters on the critical electric field.

1. Parametric study: Effect of rise time

According to Fig. 12, when the pulse width is kept constant at 10 ns, the critical electric field decreases steadily and almost linearly with increasing rise time. This reduction in electric field required is clearly due to longer "total duration" of the on time of the pulse. The figures show that the critical field is higher in case of $\lambda_o = 1.4$, indicating that for similar conditions, the confocal spheroid builds a lower TMP. As discussed before, this is essentially due to higher membrane charging times associated with spheroids. It should be noted that the critical electric field depends very weakly on the fall time, with the fall time mostly determining the relaxation of TMP, and hence, its dependence is not shown here.

2. Parametric study: Pulse width

The pulse width of the electric field determines the extent of charging of a membrane in electric field. An increase in the pulse width, results in a lower critical electric field, since the membrane is now charged for a longer time, resulting in a greater TMP. The extent of pulse width is then typically determined in terms of whether reversible or irreversible electroporation is desired as longer pulse widths can lead to larger pores and finally irreversible electroporation. Figure 13 shows the effect of pulse width on the critical field required for electroporation. At lower pulse widths, the critical field for confocal spheroidal vesicles is always greater than compound spheres due to higher charging time of the spheroids. On the other hand, when the pulse width is of the order of membrane charging time, the TMP of the spheroids is higher than that of the compound sphere system, on account of the larger size of the spheroids and hence the critical electric field for the confocal spheroids is smaller than that for compound spheres for higher pulse widths. The TMPs for the respective critical fields for compound spheres and confocal spheroids are shown in Fig. 13(b) and shows that the outer vesicle TMP is reasonable for reversible electroporation. The crossover seen in Fig. 13(a) is due to the spheroidal vesicle having

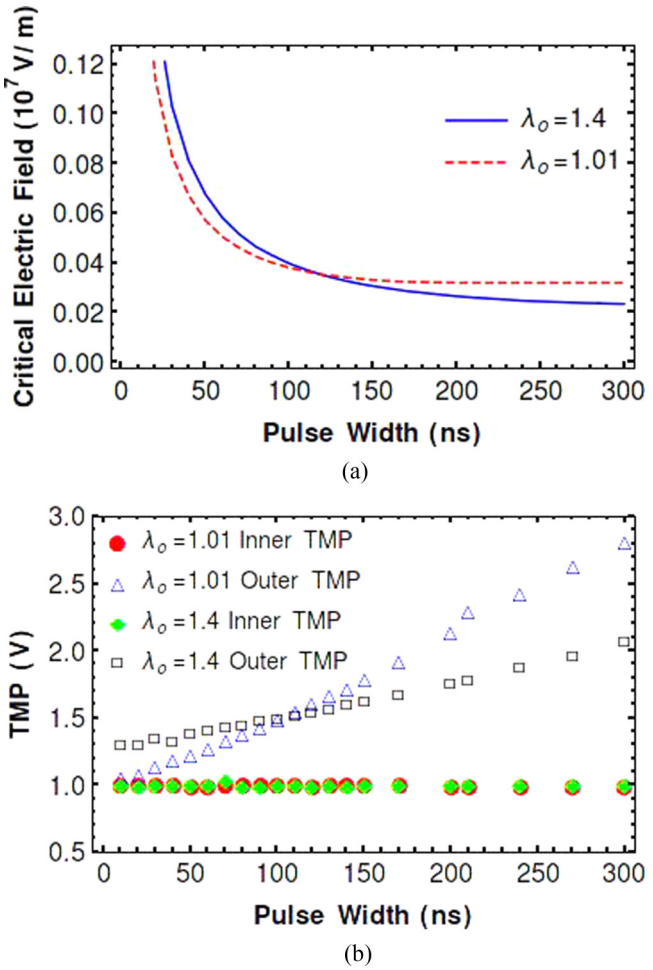

FIG. 13. The effect of pulse width on the TMP vs time response curves. (a) Variation of critical input electric field with pulse width. (b) Variation of TMP with pulse width. The parameter values are according to Tables I and II. The aspect ratio pairs are ($\lambda_o = 1.01$, $\lambda_i = 1.01$) and ($\lambda_o = 1.4$, $\lambda_i = 5$).

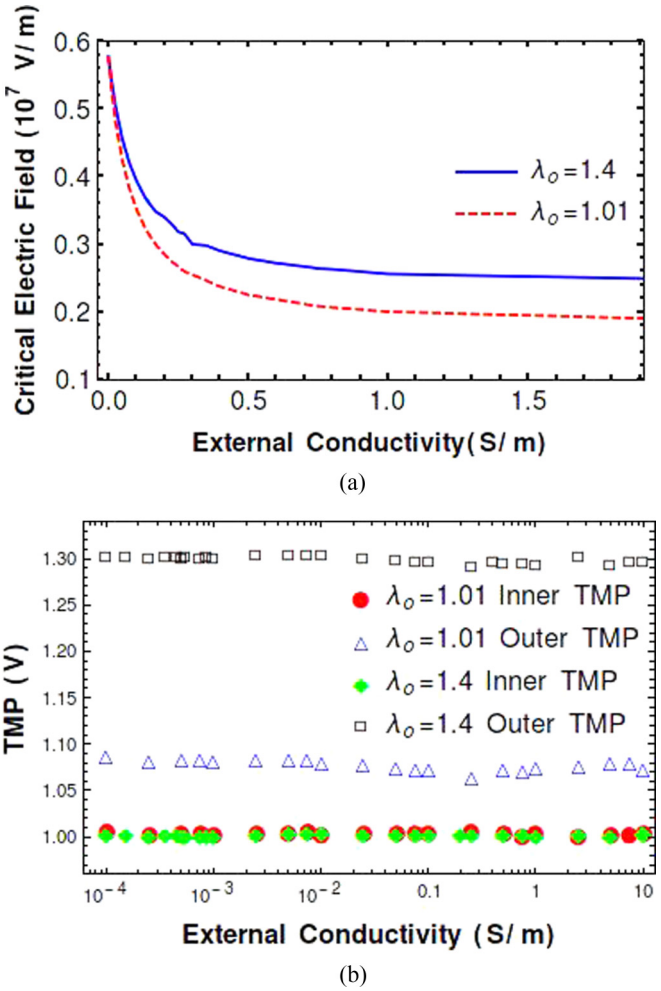

FIG. 14. Effect of external conductivity on the TMP response and critical field. (a) Variation of critical input electric field with outer medium conductivity. (b) Variation of TMP with outer medium conductivity. The physiological parameters have been taken from Tables I and II. The aspect ratio pairs are ($\lambda_o = 1.01$, $\lambda_i = 1.01$) and ($\lambda_o = 1.4$, $\lambda_i = 5$).

higher charging time and hence generating a higher saturation TMP at larger pulse widths, analogous to Fig. 6(b).

3. Parametric study: External conductivity

The critical electric field required for generating a 1V TMP in the inner vesicle decreases as the conductivity increases, due to faster charging of the membrane. The critical field is higher for confocal spheroidal vesicles as compared to concentric spherical system [Fig. 14(a)]. The critical field is nearly independent of the conductivity, at higher conductivity values, when the pulse width is much shorter than the membrane charging time.

4. Parametric study: Effect of inner membrane capacitance

The accumulation of charges at the membrane occurs over the membrane charging time which is proportional to the membrane capacitance per unit area and can be given by $C_m = \frac{\epsilon_m}{d}$. The specific membrane capacitance can be changed by changing the thickness of the membrane. In Fig. 15, the effect of the specific inner membrane capacitance, relative to a constant specific outer membrane capacitance of 0.88 μF/cm^2, is plotted, by varying the inner membrane thickness from 1 to 10 nm.

Figure 15, shows that as the membrane capacitance increases, the critical field also increases, since the higher charging time leads to slower charging of the inner membrane. With the outer capacitance remaining the same, when the inner membrane capacitance is lowered, the concentric sphere system shows a higher TMP in the inner membrane as compared to the outer, due to lower charging times of the inner vesicle. On the other hand, the confocal spheroid system seems to always exhibit a higher TMP for the outer membrane.

V. FREQUENCY DOMAIN ANALYSIS OF ECCENTRIC SPHERES

In the case of eccentric spherical compound configuration, analyzed using the bispherical coordinate system, the model

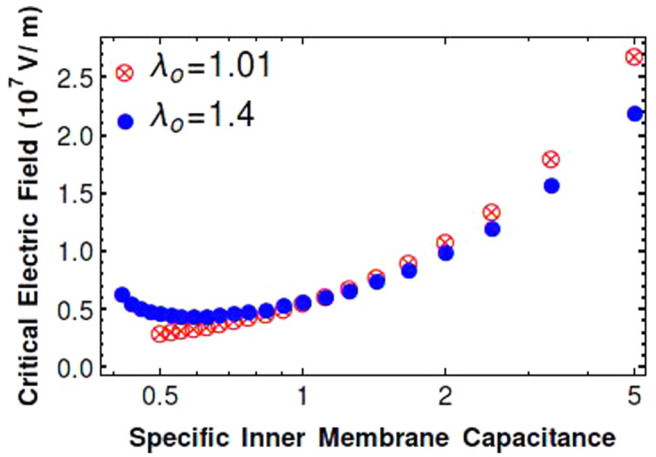

(a)

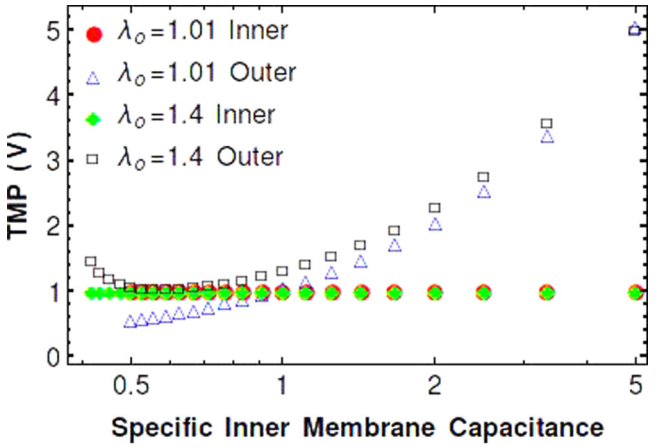

(b)

FIG. 15. Effect of specific inner membrane capacitance normalized with respect to the specific outer membrane capacitance of 0.88 μF/cm^2. (a) Variation of critical input electric field with specific inner membrane capacitance. (b) Variation of TMP with specific inner membrane capacitance. The capacitance has been varied by varying the membrane thickness through a range of thicknesses from 1 to 10 nm. The aspect ratio pairs are ($\lambda_o = 1.01$, $\lambda_i = 1.01$) and ($\lambda_o = 1.4$, $\lambda_i = 5$) and other physiological parameters are taken from Tables I and II.

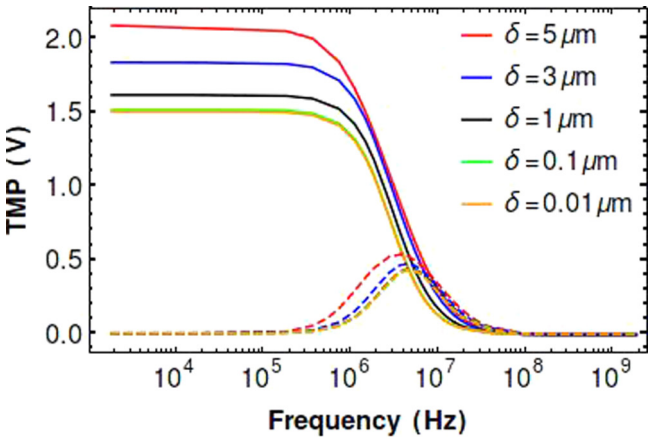

(a)

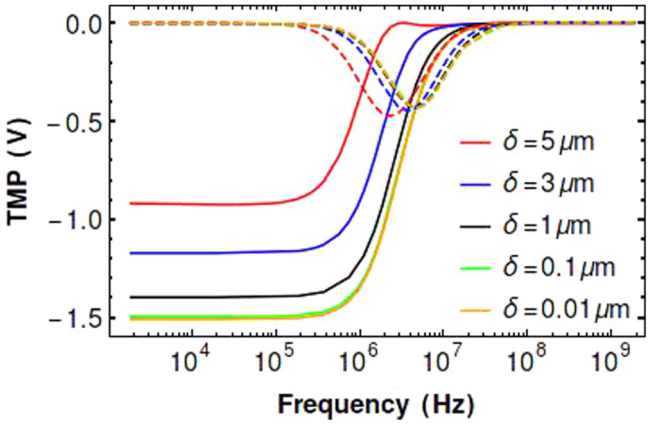

(b)

FIG. 16. Effect of offset on TMP at both poles. (a) Variation of TMP with frequency at the north pole. (b) Variation of TMP with frequency at the south pole. The solid lines represent the outer TMP and the dashed lines represent the inner TMP, with $E_o = 1$ kV/cm. The geometrical and electrical parameters are from Tables I and II.

for the eccentric vesicle, where the nucleus or the organelles are offset from the center, but spherical in shape, frequency domain analysis is used for an analytical treatment of the system.

A. Effect of offset

The eccentricity of the inner vesicle (representing the nucleus) in a compound spherical system is expected to cause deviations of the TMP from the concentric sphere case and these variations (Fig. 16) are clearly seen in the peak values at the two poles of the inner vesicle, where the offset (eccentricity) results in significant stretching or contraction of the TMP vs frequency curve. Figure 16 shows that the offset causes a significant change in the peak TMP values in both the inner and the outer vesicles. The TMP at the south pole (Fig. 2) decreases with an increase in the offset. On the other hand the TMP of the north pole increases with an increase in offset. Thus the north pole is more likely to get porated as compared to the south pole, indicating that in a nsPEF operation, the vesicle will experience a greater influx of ionic material, coming into the cytoplasm, at the north pole. This will correspondingly result in greater probability of ingression of ionic species at the north pole of the nuclear (inner) membrane as well. The inner membrane shows very little influence of the offset. A marked difference is only visible at offsets which are of the same order as the size of the system, where the TMP in the inner membrane increases slightly at the north pole and decreases slightly at the south pole. This appears a bit counterintutive since a field convergence is expected near the south pole. This is indeed observed in calculations (not shown in the article) where the absolute values of the potentials at the inner and outer leaflets of the bilayer membrane at south pole are significantly higher than those at the north pole. However, the difference between the potentials of the inner and the outer leaflets, which is termed the TMP, is higher at the north pole than the south pole.

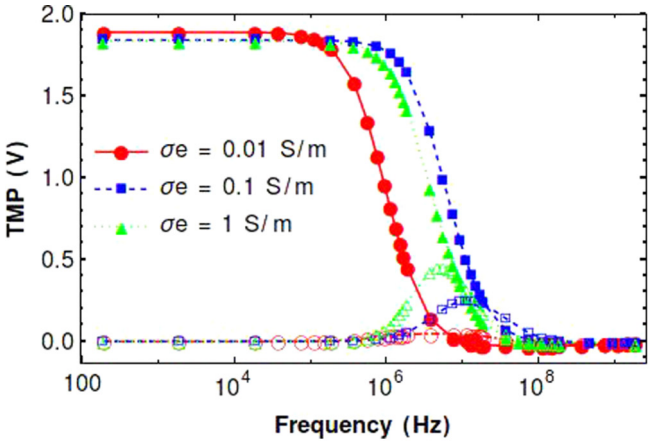

(a)

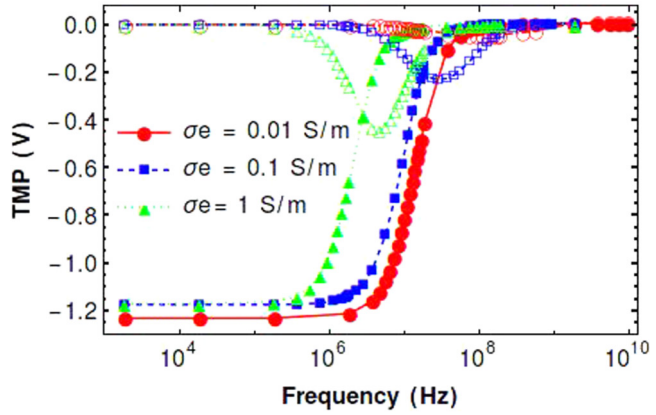

(b)

FIG. 17. Effect of outer medium conductivity on TMP for an offset of 3 μm and $E_o = 1$ kV/cm. (a) Variation of TMP with frequency at the north pole. (b) Variation of TMP with frequency at the south pole. Conductivity values are in S/m. The other parameters are from Tables II and I. Filled markers are for outer TMP and empty markers denote inner TMP.

B. Effect of outer medium conductivity

The effect of outer membrane conductivity is investigated for eccentric vesicles with an offset of 3 μm (Fig. 17) and it is seen that outer medium conductivity significantly affects both the TMPs. With increasing conductivity, the charging time decreases and thus the curves shift to the right, with negligible effect on the maximum value of the outer TMP. For low conductivities ($\leqslant 10^{-2}$), the TMP across the inner membrane is very small and it decreases monotonically with medium conductivity. However, there is no fixed trend and the effect of conductivity on the south pole TMP needs further investigation as it seems to respond faster than the north pole.

VI. FINITE ELEMENT CALCULATIONS OF ECCENTRIC COMPOUND SPHERICAL VESICLE

For bispherical geometry, it is difficult to have a mathematical framework for dc pulses due to the complexity in converting from Laplace domain to time domain in bispherical geometry, unlike in the case of spheroidal vesicles where elegant analytical treatment is possible. Hence, instead, COMSOL Multiphysics simulations have been carried out for both ac and dc inputs. Simulation results have been tested against analytical results obtained for ac fields to establish further that the methods used in this work are satisfactory. The simulations are then extended to conduct further analysis in the dc domain. The maximum element size is taken as 3.35 μm and the minimum as 1 nm, with a curvature factor of 0.3. The time step for simulation is $t_0/2500$ where t_0 is the time to which simulations have been run. It should be noted that although the results improve on making the discretization grid finer, increasing the mesh size beyond a certain point does not yield any better data. Moreover, the time steps and the mesh size have to be tuned together. The domain of the membranes does not require extensive meshing and only mesh points at the boundary of the domain seem to suffice. This is because the membrane is very thin (5 nm), as compared to the size of the vesicle (around 5–10 μm) and a linear variation is not fallacious.

Comparison between analytical theory and COMSOL simulations for compound spheroids were carried out for vesicles subjected to dc pulse (as discussed in the earlier sections) and a satisfactory agreement is observed between theory and simulation. In addition to the above, comparison between results obtained from analytical theory and finite-element simulations for eccentric compound spheres subjected to ac fields were also undertaken and the general trend were found to be in agreement [46]. COMSOL simulations for concentric and eccentric compound spherical vesicle subjected to a dc pulse input have been presented in this paper. It is observed that the offset in the eccentric compound spherical vesicle has a significant effect on the TMP evolution in the vesicle. The dc response for trapezoidal pulses for different offsets is presented in Fig. 18 and the same trend as seen in the frequency domain also gets reflected here. For both the outer and the inner vesicles, the south pole TMP decreases with offset while an increase in TMP with offset is observed for the north pole TMP. However the variation of the north pole TMP for the outer membrane appears to show an extrema with the offset as seen in Fig. 18(d). It is seen that a 3-μm offset vesicle has the highest TMP distribution, as opposed to the other cases where the TMP shifts uniformly with the offset and the 5-μm offset vesicle has the highest TMP values. Thus, for the north pole outer membrane, the maximum TMP as a function of the offset has an extrema, while in the other figures, it is an increasing function. As argued earlier, the enhancement of TMP at the north pole is due to a greater difference between the potentials at the inner and the outer leaflets of the inner vesicle, although the absolute values of leaflet potentials for the north pole are smaller than the corresponding values at the south pole. An asymmetry in the TMP is also seen in literature, as seen by Frey *et al.* [47]; however, their experiments seem to have the nonaxisymmetric eccentricity and hence, the exact cause of the asymmetry in the TMP distribution cannot be attributed to the eccentricity of the nucleus with certainty. The shifts in the TMP is also much more pronounced in the south pole than the north pole. An effort to fit the maximum nondimensional TMP as a function of the nondimensional offset is carried out and it is seen, that

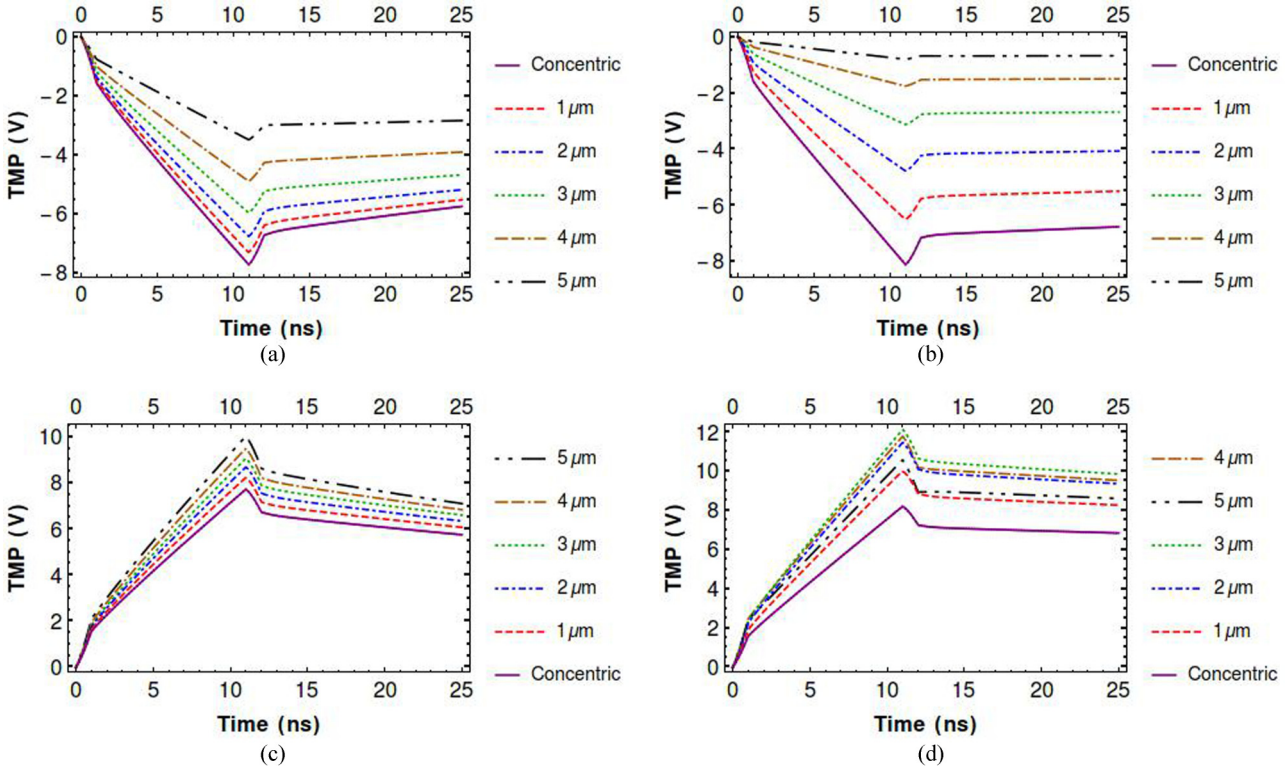

FIG. 18. TMP vs time curves response, from simulation for eccentric vesicles subjected to nsPEF, for different offsets. (a) Inner TMP South Pole. (b) Outer TMP South Pole. (c) Inner TMP North Pole. (d) Outer TMP North Pole. The electrical and geometrical parameter values have been taken from Tables I and II.

linear and quadratic polynomials give a very good fit with the simulation data as seen in Fig. 19.

VII. CONCLUSION

The analysis on confocal spheroidal vesicles suggests the critical electric field required in spheroidal vesicles, as compared to spherical vesicles, is higher under nsPEFs, but lower for longer pulse widths of micro- to millisecond range, where the spheroidal vesicles develop a higher saturation TMP. It is suggested that the requirement of the higher critical electric field is due to the larger effective radius of the spheroidal vesicle and thereby larger membrane charging time. Once the critical electric field, in the nsPEF regime, builds the threshold TMP, it may be required to hold the TMP at a desired value for a desired time period, or to reduce it to zero instantaneously. This is critical to control the poration mechanics, the pore distribution and pore radius, especially so in nsPEF where the field strengths are orders of magnitude higher than those in msPEF and μsPEF. In order to have better control over the temporal distribution, bipolar pulses, or trains of bipolar pulses, can be used to great advantage, as the relative magnitude and separation of the two pulses can sustain or annihilate the TMP, as required. For msPEF and μsPEF, where the membrane could be completely charged, the external conductivity does not have a marked effect on the saturation value of the TMP. However, for nsPEFs, where the pulse durations are always lower than the membrane charging time, the conductivity plays an important role, and due to the coupling between the outer and the inner membranes, the external conductivity influences the inner TMP, despite the charging time of the inner vesicle remaining the same. TMP also depends sensitively on the membrane capacitances, such that organelles with lower capacitances are easier to porate. The mitochondrial and nuclear membranes can generally be thicker than the cell membrane, and thus, the TMP across them can, in fact, exceed that of the cell membrane.

The eccentric model reveals some interesting features, namely the lowering and raising of the TMP due to the eccentricity, at the south and north poles, respectively. The lowering of the TMP, due to the close approach of the nucleus to the outer cell membrane in a nucleate cell is an interesting feature and merits further investigation into the phenomenon. The analytical method presented in this study for solving Laplace equations for particular solutions in the bispherical coordinate can be used for benchmarking in future studies. The method is not restricted to any particular case and can be used in any such problems, for instance, to solve for electrofusion of vesicles or electrocoalescence of droplets under electric fields.

FEM calculations using COMSOL were rigorously validated with analytical theory and also establishes the FEM parameters for the TMP calculations for electroporation. These can then be customized and is expected to be specific to the system configuration.

Bilayer membrane vesicles, such as assumed in this study, are popular biomimetic constructs which are used to understand various phenomenon in real biological cells. However,

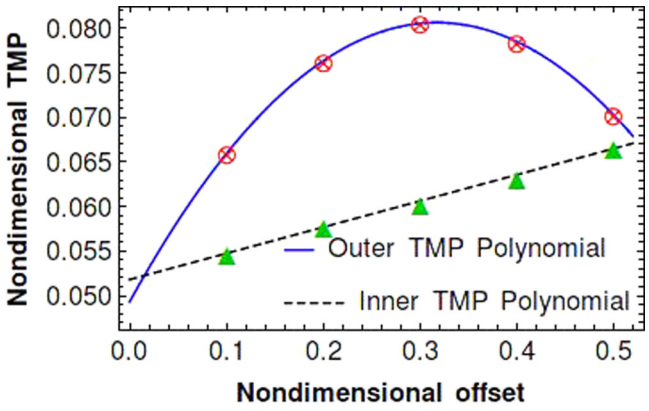

(a)

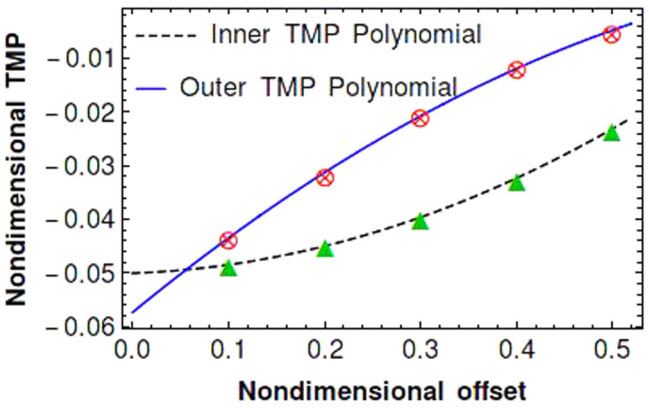

(b)

FIG. 19. Curve-fitting of maximum nondimensional TMP as a function of the nondimensional offset. (a) Nondimensional TMP vs nondimensional offset for north pole. (b) Nondimensional TMP vs nondimensional offset for south pole. The solid lines represent the TMP across the outer (plasma) membrane, while the dashed lines represent that across the inner (nuclear) membrane, both obtained from fitting the data to a curve (either linear or quadratic). The crossed circles and solid triangles, on both the figures, represent points obtained from simulation, which have been used to fit the curves.

there are major differences between such cells and vesicles, due the structural complexity of the cell membrane, and hence, the mechanisms in real cells are also far more complicated. Complex protein channels embedded in the membranes can open or close, depending on the TMP, and under voltages much smaller than the TMP, they can admit flow of current through the membrane. However, this small flow of current does not not lower the TMP [48]. Notably, the kinetics of vesicles are much faster than those observed in biological cells, by orders of 1000. The restructuring of the cytoskeleton framework of the cell membranes are thought to have a marked effect on the pore dynamics, with delayed pore formation taking place. Cytoskeletal disruption has been shown to strongly influence the TMP [49] and prevent cell death [50].

It should be mentioned here that the treatment presented in this work considers unelectroporated membranes, thereby enabling an axisymmetric approach. However, when the bilayer is electroporated when the TMP exceeds the threshold value, the electrostatic boundary conditions used in Eqs. (16)–(19) could change significantly [51] and the membrane conductance term can no longer be ignored. The membrane conductance in fact is now dependent on the pore size, pore density, pore distribution and the conductivities of the inner and outer medium. This enhancement in membrane conductance due to electroporation can change the electrostatics as well as the TMP distribution on the membrane surface and is ignored in the present analysis. The poration is typically nonaxisymmetric and the problem therefore would be rendered nonaxisymmetric as well. The present analysis is certainly valid at the onset of electroporation. Moreover, for TMP just above the threshold values, one could expect that the membrane conductance is not significantly altered, thereby suggesting that the results of the present analysis could be still valid in the experiments.

ACKNOWLEDGMENT

The authors thank the Department of Science and Technology, India, for financial support.

APPENDIX A: RESTRICTION ON INNER ASPECT RATIO IN CONFOCAL SPHEROIDAL SYSTEMS

The semifocal length ($c = a/\xi$, $\xi = \frac{\lambda}{\sqrt{\lambda^2-1}}$), calculated from the inner and outer aspect ratios must be the same for confocal spheroidal vesicles and this fact gives rise to the geometric constraints on the dimensions of the inner spheroid. Equating the volume of a spheroid and sphere,

$$\tfrac{4}{3}\pi ab^2 = \tfrac{4}{3}\pi r^3, \tag{A1}$$

$$\Rightarrow a = r\left(\frac{a}{b}\right)^{\frac{2}{3}}, \tag{A2}$$

$$\Rightarrow a = r(\lambda)^{\frac{2}{3}}. \tag{A3}$$

Thus, equating the semifocal length from both inner and outer aspect ratios,

$$\frac{R_o\left(\lambda_o^{\frac{2}{3}}\right)\sqrt{\lambda_o^2-1}}{\lambda_o} = \frac{R_i\left(\lambda_i^{\frac{2}{3}}\right)\sqrt{\lambda_i^2-1}}{\lambda_i}, \tag{A4}$$

$$\Rightarrow (\lambda_i)^{\frac{4}{3}}\left(1-\frac{1}{\lambda_i^2}\right) = \frac{R_o^2}{R_i^2}\lambda_o^{\frac{4}{3}}\left(1-\frac{1}{\lambda_o^2}\right). \tag{A5}$$

One can use inner aspect ratio values which are higher than those obtained from this equation, but never values which are smaller.

APPENDIX B: EQUATIONS AND SOLUTION METHODOLOGY FOR BISPHERICAL SYSTEM FOR ECCENTRIC COMPOUND SPHERICAL VESICLES

After solving the Laplace equation in bispherical coordinates and applying the far field and consistency conditions, the potential equations are given below. Let $H_m^+(\xi) \equiv e^{(m+\frac{1}{2})\xi}$, $H_m^-(\xi) \equiv e^{-(m+\frac{1}{2})\xi}$, and $P_m(\cos\eta) \equiv P_m(\eta)$:

$$\phi_n = (\cosh\xi - \cos\eta)^{\frac{1}{2}}\left[\Sigma_{m=0}^{\infty} P_m(\eta)\, a_m H_m^-(\xi)\right], \tag{B1}$$

$$\phi_{\rm nm} = (\cosh\xi - \cos\eta)^{\frac{1}{2}}\left\{\Sigma_{m=0}^{\infty} P_m(\eta)\,[b_m H_m^+(\xi) + c_m H_m^-(\xi)]\right\}, \tag{B2}$$

$$\phi_c = (\cosh\xi - \cos\eta)^{\frac{1}{2}}\left\{\Sigma_{m=0}^{\infty} P_m(\eta)\,[d_m H_m^+(\xi) + e_m H_m^-(\xi)]\right\}, \tag{B3}$$

$$\phi_{\rm cm} = (\cosh\xi - \cos\eta)^{\frac{1}{2}}\left\{\Sigma_{m=0}^{\infty} P_m(\eta)\,[f_m H_m^+(\xi) + g_m H_m^-(\xi)]\right\}, \tag{B4}$$

$$\phi_e = (\cosh\xi - \cos\eta)^{\frac{1}{2}}\left\{\Sigma_{m=0}^{\infty} P_m(\eta)\left[j_m H_m^+(\xi) - \frac{c}{R_o}\sqrt{2}(2m+1)H_m^-(\xi)\right]\right\}. \tag{B5}$$

The formulation for the equations in bispherical coordinates have been shown here for the interface between the nucleus and the nuclear membrane. From potential continuity,

$$\phi_n(\xi_1,\eta) = \phi_{\rm nm}(\xi_1,\eta) \Rightarrow \sum_{m=0}^{\infty} P_m(\eta) a_m H_m^-(\xi_1) = \sum_{m=0}^{\infty} P_m(\eta)[b_m H_m^+(\xi_1) + c_m H_m^-(\xi_1)]$$

$$\Rightarrow \sum_{m=0}^{\infty} P_m(\eta)[a_m H_m^-(\xi_1) - b_m H_m^+(\xi_1) - c_m H_m^-(\xi_1)] = 0$$

and by linear independence of $P_m(\eta)$

$$a_m = b_m H_m^+(\xi_1)^2 + c_m. \tag{B6}$$

The current continuity, Eq. (16), becomes

$$K_n \overline{\nabla}\phi_n \cdot \hat{\xi}|_{\xi=\xi_1} = K_{\rm nm}\overline{\nabla}\phi_{\rm nm}\cdot\hat{\xi}|_{\xi=\xi_1} \Rightarrow K_n \frac{\partial\phi_n}{\partial\xi}|_{\xi=\xi_1} = K_{\rm nm}\frac{\partial\phi_{\rm nm}}{\partial\xi}|_{\xi=\xi_1} \Rightarrow K_n \sinh\xi_1 \sum_{m=0}^{\infty} P_m(\eta) a_m H_m^-(\xi_1)$$

$$- K_n(\cosh\xi_1 - \cos\eta)\sum_{m=0}^{\infty} P_m(\eta)(2m+1)a_m H_m^-(\xi_1)$$

$$= K_{\rm nm}\sinh\xi_1 \sum_{m=0}^{\infty} P_m(\eta)[b_m H_m^+(\xi_1) + c_m H_m^-(\xi_1)]$$

$$+ K_{\rm nm}(\cosh\xi_1 - \cos\eta)\sum_{m=0}^{\infty} P_m(\eta)(2m+1)[b_m H_m^+(\xi_1) - c_m H_m^-(\xi_1)]$$

$$\Rightarrow \sinh\xi_1 \sum_{m=0}^{\infty} P_m(\eta)\{K_n a_m H_m^-(\xi_1) - K_{\rm nm}[b_m H_m^+(\xi_1) + c_m H_m^-(\xi_1)]\}$$

$$- (\cosh\xi_1 - \cos\eta)\sum_{m=0}^{\infty} P_m(\eta)(2m+1)\{K_n a_m H_m^-(\xi_1) + K_{\rm nm}[b_m H_m^+(\xi_1) - c_m H_m^-(\xi_1)]\} = 0\cdots \tag{B7}$$

A substitution has been made here by taking

$$\alpha_m = K_n[b_m H_m^+(\xi_1) + c_m H_m^-(\xi_1)] - K_{\rm nm}[b_m H_m^+(\xi_1) + c_m H_m^-(\xi_1)]$$

$$\beta_m = K_n[b_m H_m^+(\xi_1) + c_m H_m^-(\xi_1)] + K_{\rm nm}[b_m H_m^+(\xi_1) - c_m H_m^-(\xi_1)] \tag{B8}$$

and the following form of an equation under the summation sign is obtained:

$$\sinh\xi_1 \sum_{m=0}^{\infty} P_m(\eta)\alpha_m + \sum_{m=0}^{\infty} P_m(2m+1)(\cos\eta - \cosh\xi_1)\beta_m = 0.$$

The recurrence relation for Legendre polynomials has been used

$$xP_m(x)(2m+1) = (m+1)P_{m+1}(x) + mP_{m-1}(x)$$

to get the equation

$$\sinh\xi_1 \sum_{m=0}^{\infty} P_m(\eta)\alpha_m - \cosh\xi_1 \sum_{m=0}^{\infty} P_m(\eta)(2m+1)\beta_m + \sum_{m=0}^{\infty}(m+1)P_{m+1}(\eta)\beta_m + \sum_{m=0}^{\infty} mP_{m-1}(\eta)\beta_m = 0. \tag{B9}$$

Replacing $m+1$ by n in the third term and $m-1$ by n in the last term, the following difference equation can be obtained:

$$\sinh\xi_1 \sum_{m=0}^{\infty} P_m(\eta)\alpha_m - \cosh\xi_1 \sum_{m=0}^{\infty} P_m(\eta)(2m+1)\beta_m + \sum_{n=1}^{\infty} nP_n(\eta)\beta_{n-1} + \sum_{n=-1}^{\infty}(n+1)P_n(\eta)\beta_{n+1} = 0.$$

In the third term, the summation can be taken from $n=0$ as the resulting term is zero and will not affect the equation. Similarly, the last term can be taken from $n=0$ as for $n=-1$, the resulting term is zero and does not contribute. Thus appropriately adjusting the lower limit of the index and replacing all the n's by m, the following equation can be obtained,

$$\sinh\xi_1 \sum_{m=0}^{\infty} P_m(\eta)\alpha_m - \cosh\xi_1 \sum_{m=0}^{\infty} P_m(\eta)(2m+1)\beta_m + \sum_{m=0}^{\infty} mP_m(\eta)\beta_{m-1} + \sum_{m=0}^{\infty}(m+1)P_m(\eta)\beta_{m+1} = 0, \tag{B10}$$

and from linear independence of the Legendre polynomials in η, the final form of Eq. (34) can be obtained:

$$\sinh\xi_1\alpha_m - \cosh\xi_1(2m+1)\beta_m + m\beta_{m-1} + (m+1)\beta_{m+1} = 0 \tag{B11}$$

in which, the variables are b_m and c_m. Similarly, for the other boundary conditions, the same method can be applied to yield the following set of equations:

$$\begin{aligned}
\sinh\xi_2\gamma_m + \cosh\xi_2(2m+1)\delta_m - m\delta_{m-1} - (m+1)\delta_{m+1} &= 0\\
\sinh\xi_3\tau_m + \cosh\xi_3(2m+1)\chi_m - m\chi_{m-1} - (m+1)\chi_{m+1} &= 0\\
\sinh\xi_4\rho_m + \cosh\xi_4(2m+1)\mu_m - m\mu_{m-1} - (m+1)\mu_{m+1} &= 0
\end{aligned} \tag{B12}$$

with variables b_m, c_m, g_m, j_m after replacing variables a_m, d_m, e_m, f_m from potential continuity equations. The system of equations can be written in a matrix form for some fixed value of m (say, n). Following the formulation in the previous section, the set of equations are

$$\begin{aligned}
&A_{1,m}b_m + A_{2,m}c_m + A_{3,m}g_m + A_{4,m}j_m + A_{5,m}b_{m-1} + A_{6,m}c_{m-1} + A_{7,m}g_{m-1}\\
&\quad + A_{8,m}j_{m-1} + A_{9,m}b_{m+1} + A_{10,m}c_{m+1} + A_{11,m}g_{m+1} + A_{12,m}j_{m+1} = 0\\
&B_{1,m}b_m + B_{2,m}c_m + B_{3,m}g_m + B_{4,m}j_m + B_{5,m}b_{m-1} + B_{6,m}c_{m-1} + B_{7,m}g_{m-1}\\
&\quad + B_{8,m}j_{m-1} + B_{9,m}b_{m+1} + B_{10,m}c_{m+1} + B_{11,m}g_{m+1} + B_{12,m}j_{m+1} = 0\\
&C_{1,m}b_m + C_{2,m}c_m + C_{3,m}g_m + C_{4,m}j_m + C_{5,m}b_{m-1} + C_{6,m}c_{m-1} + C_{7,m}g_{m-1}\\
&\quad + C_{8,m}j_{m-1} + C_{9,m}b_{m+1} + C_{10,m}c_{m+1} + C_{11,m}g_{m+1} + C_{12,m}j_{m+1} = 0\\
&D_{1,m}b_m + D_{2,m}c_m + D_{3,m}g_m + D_{4,m}j_m + D_{5,m}b_{m-1} + D_{6,m}c_{m-1} + D_{7,m}g_{m-1} + D_{8,m}j_{m-1}\\
&\quad + D_{9,m}b_{m+1} + D_{10,m}c_{m+1} + D_{11,m}g_{m+1} + D_{12,m}j_{m+1} = 0
\end{aligned} \tag{B13}$$

with $m=0$ to n. For $m=0$, the coefficients corresponding to $b_{-1},\ c_{-1},\ g_{-1},\ j_{-1}$ turn out to be zero and thus we do not get constants with negative coefficients. The system matrix can be written as shown below. As the index m runs from 0 to n, a set of $4(n+1)$ equations are obtained from four difference equations corresponding to each m, and a set of $4(n+2)$ variables. The method expounded in this paper is to set to zero, the $(n+1)$th variables, arguing that for a convergent solution, with increasing value of n, the higher harmonics will have progressively lesser contributions and thus, the final four coefficients are dropped

leading to $4(n+1)$ equations in $4(n+1)$ variables, which can be solved:

$$\begin{pmatrix}
A_{1,0} & A_{2,0} & A_{3,0} & A_{4,0} & A_{9,0} & A_{10,0} & A_{11,0} & A_{12,0} & 0\,0\,0.... & & & & \\
B_{1,0} & B_{2,0} & B_{3,0} & B_{4,0} & B_{9,0} & B_{10,0} & B_{11,0} & B_{12,0} & 0\,0\,0.... & & & & \\
C_{1,0} & C_{2,0} & C_{3,0} & C_{4,0} & C_{9,0} & C_{10,0} & C_{11,0} & C_{12,0} & 0\,0\,0.... & & & & \\
D_{1,0} & D_{2,0} & D_{3,0} & D_{4,0} & D_{9,0} & D_{10,0} & D_{11,0} & D_{12,0} & 0\,0\,0.... & & & & \\
A_{5,1} & A_{6,1} & A_{7,1} & A_{8,1} & A_{1,1} & A_{2,1} & A_{3,1} & A_{4,1} & A_{9,1} & A_{10,1} & A_{11,1} & A_{12,1} & 0\,0\,0.... \\
. & & & & & & & & & & & & \\
. & & & & & & & & & & & & \\
. & & & & & & & & & & & & \\
..0\,0 & A_{5,n} & A_{6,n} & A_{7,n} & A_{8,n} & A_{1,n} & A_{2,n} & A_{3,n} & A_{4,n} & A_{9,n} & A_{10,n} & A_{11,n} & A_{12,n} \\
. & & & & & & & & & & & & \\
. & & & & & & & & & & & & \\
..0\,0 & D_{5,n} & D_{6,n} & D_{7,n} & D_{8,n} & D_{1,n} & D_{2,n} & D_{3,n} & D_{4,n} & D_{9,n} & D_{10,n} & D_{11,n} & D_{12,n}
\end{pmatrix}
\begin{pmatrix}
b_0 \\ c_0 \\ g_0 \\ j_0 \\ b_1 \\ c_1 \\ g_1 \\ j_1 \\ b_2 \\ c_2 \\ g_2 \\ j_2 \\ . \\ . \\ . \\ b_{n-1} \\ c_{n-1} \\ g_{n-1} \\ j_{n-1} \\ b_n \\ c_n \\ g_n \\ j_n \\ b_{n+1} \\ c_{n+1} \\ g_{n+1} \\ j_{n+1}
\end{pmatrix}
=
\begin{pmatrix}
0 \\ 0 \\ 0 \\ 0 \\ 0 \\ 0 \\ 0 \\ 0 \\ 0
\end{pmatrix}.$$

The final matrix system looks as shown below. It should be remembered that the value of n is a matter of trial and error and it varies from one problem to another.

$$\begin{pmatrix}
A_{1,0} & A_{2,0} & A_{3,0} & A_{4,0} & A_{9,0} & A_{10,0} & A_{11,0} & A_{12,0} & 0\,0\,0.... & & & & \\
B_{1,0} & B_{2,0} & B_{3,0} & B_{4,0} & B_{9,0} & B_{10,0} & B_{11,0} & B_{12,0} & 0\,0\,0.... & & & & \\
C_{1,0} & C_{2,0} & C_{3,0} & C_{4,0} & C_{9,0} & C_{10,0} & C_{11,0} & C_{12,0} & 0\,0\,0.... & & & & \\
D_{1,0} & D_{2,0} & D_{3,0} & D_{4,0} & D_{9,0} & D_{10,0} & D_{11,0} & D_{12,0} & 0\,0\,0.... & & & & \\
A_{5,1} & A_{6,1} & A_{7,1} & A_{8,1} & A_{1,1} & A_{2,1} & A_{3,1} & A_{4,1} & A_{9,1} & A_{10,1} & A_{11,1} & A_{12,1} & 0\,0.... \\
B_{5,1} & B_{6,1} & B_{7,1} & B_{8,1} & B_{1,1} & B_{2,1} & B_{3,1} & B_{4,1} & B_{9,1} & B_{10,1} & B_{11,1} & B_{12,1} & 0\,0.... \\
C_{5,1} & C_{6,1} & C_{7,1} & C_{8,1} & C_{1,1} & C_{2,1} & C_{3,1} & C_{4,1} & C_{9,1} & C_{10,1} & C_{11,1} & C_{12,1} & 0\,0.... \\
D_{5,1} & D_{6,1} & D_{7,1} & D_{8,1} & D_{1,1} & D_{2,1} & D_{3,1} & D_{4,1} & D_{9,1} & D_{10,1} & D_{11,1} & D_{12,1} & 0\,0.... \\
. & & & & & & & & & & & & \\
. & & & & & & & & & & & & \\
. & & & & & & & & & & & & \\
..0\,0 & A_{5,n} & A_{6,n} & A_{7,n} & A_{8,n} & A_{1,n} & A_{2,n} & A_{3,n} & A_{4,n} & A_{9,n} & A_{10,n} & A_{11,n} & A_{12,n} \\
. & & & & & & & & & & & & \\
. & & & & & & & & & & & & \\
..0\,0 & D_{5,n} & D_{6,n} & D_{7,n} & D_{8,n} & D_{1,n} & D_{2,n} & D_{3,n} & D_{4,n} & D_{9,n} & D_{10,n} & D_{11,n} & D_{12,n}
\end{pmatrix}
\begin{pmatrix}
b_0 \\ c_0 \\ g_0 \\ j_0 \\ b_1 \\ c_1 \\ g_1 \\ j_1 \\ b_2 \\ c_2 \\ g_2 \\ j_2 \\ . \\ . \\ . \\ b_{n-1} \\ c_{n-1} \\ g_{n-1} \\ j_{n-1} \\ b_n \\ c_n \\ g_n \\ j_n
\end{pmatrix}
=
\begin{pmatrix}
0 \\ 0 \\ 0 \\ 0 \\ 0 \\ 0 \\ 0 \\ 0 \\ 0
\end{pmatrix}.$$

[1] G. Narayanan, Irreversible electroporation for treatment of liver cancer, Gastroenterol. Hepatol. **7**, 313 (2011).

[2] I. Abidor, V. Arakelyan, L. Chernomordik, Y. A. Chizmadzhev, V. Pastushenko, and M. Tarasevich, Electric breakdown of bilayer lipid membranes: I. The main experimental facts and their qualitative discussion, J. Electroanal. Chem. Interfacial Electrochem. **104**, 37 (1979).

[3] S. J. Beebe, J. White, P. F. Blackmore, Y. Deng, K. Somers, and K. H. Schoenbach, Diverse effects of nanosecond pulsed electric fields on cells and tissues, DNA Cell Biol. **22**, 785 (2003).

[4] E. B. Garon, D. Sawcer, P. T. Vernier, T. Tang, Y. Sun, L. Marcu, M. A. Gundersen, and H. P. Koeffler, In vitro and in vivo evaluation and a case report of intense nanosecond pulsed electric field as a local therapy for human malignancies, In. J. Cancer **121**, 675 (2007).

[5] J. C. Weaver, K. C. Smith, A. T. Esser, R. S. Son, and T. Gowrishankar, A brief overview of electroporation pulse strength–duration space: A region where additional intracellular effects are expected, Bioelectrochem. **87**, 236 (2012).

[6] K. H. Schoenbach, S. J. Beebe, and E. S. Buescher, Intracellular effect of ultrashort electrical pulses, Bioelectromagnetics **22**, 440 (2001).

[7] R. Dimova, K. A. Riske, S. Aranda, N. Bezlyepkina, R. L. Knorr, and R. Lipowsky, Giant vesicles in electric fields, Soft Matter **3**, 817 (2007).

[8] A. Denzi, E. della Valle, G. Esposito, L. M. Mir, F. Apollonio, and M. Liberti, Technological and theoretical aspects for testing electroporation on liposomes, BioMed Res. Int. **2017**, 5092704 (2017).

[9] S. Aranda, K. A. Riske, R. Lipowsky, and R. Dimova, Morphological transitions of vesicles induced by alternating electric fields, Biophys. J. **95**, L19 (2008).

[10] H. Hyuga, K. Kinosita, Jr., and N. Wakabayashi, Deformation of vesicles under the influence of strong electric fields, Jpn. J. Appl. Phys. **30**, 1141 (1991).

[11] T. Yoshida, H. Okuyama, H. Endo, and M. Inoue, Spheroid cultures of primary urothelial cancer cells: Cancer tissue-originated spheroid (ctos) method, in *Urothelial Carcinoma* (Springer, New York, 2018), pp. 145–153.

[12] G. Cheng, R. Lanning, D. Fukumura, R. Jain, and L. Munn, Mechanical stress affects tumor spheroid shape and cell phenotype, American Association for Cancer Research **68**, 435 (2008).

[13] M. Wu, T. Tu, Y. Huang, and Y. Cao, Suppression subtractive hybridization identified differentially expressed genes in lung adenocarcinoma: Ergic3 as a novel lung cancer-related gene, BMC Cancer **13**, 44 (2013).

[14] Q. Hu and R. P. Joshi, Transmembrane voltage analyses in spheroidal cells in response to an intense ultrashort electrical pulse, Phys. Rev. E **79**, 011901 (2009).

[15] H. Nganguia and Y.-N. Young, Equilibrium electrodeformation of a spheroidal vesicle in an ac electric field, Phys. Rev. E **88**, 052718 (2013).

[16] R. P. Joshi and J. Song, Model analysis of electric fields induced by high-voltage pulsing in cylindrical nerves, IEEE Trans. Plasma Sci. **38**, 2894 (2010).

[17] M. Klee and R. Plonsey, Stimulation of spheroidal cells-the role of cell shape, IEEE Trans. Biomed. Eng. **BME-23**, 347 (1976).

[18] C. Yao, X. Hu, Y. Mi, C. Li, and C. Sun, Window effect of pulsed electric field on biological cells, IEEE Trans. Dielectr. Electr. Insul. **16**, 1259 (2009).

[19] T. Kotnik and D. Miklavčič, Theoretical evaluation of voltage inducement on internal membranes of biological cells exposed to electric fields, Biophys. J. **90**, 480 (2006).

[20] C. Yao, D. Mo, C. Li, C. Sun, and Y. Mi, Study of transmembrane potentials of inner and outer membranes induced by pulsed-electric-field model and simulation, IEEE Trans. Plasma Sci. **35**, 1541 (2007).

[21] T. Kotnik, D. Miklavčič, and T. Slivnik, Time course of transmembrane voltage induced by time-varying electric fieldsa method for theoretical analysis and its application, Bioelectrochem. Bioenerg. **45**, 3 (1998).

[22] T. Kotnik and D. Miklavčič, Analytical description of transmembrane voltage induced by electric fields on spheroidal cells, Biophys. J. **79**, 670 (2000).

[23] Q. Hu and R. P. Joshi, Analysis of intense, subnanosecond electrical pulse-induced transmembrane voltage in spheroidal cells with arbitrary orientation, IEEE Trans. Biomed. Eng. **56**, 1617 (2009).

[24] A. Goyette and A. Navon, Two dielectric spheres in an electric field, Phys. Rev. B **13**, 4320 (1976).

[25] M. H. Davis, Two charged spherical conductors in a uniform electric field: Forces and field strength, Q. J. Mech. Appl. Math. **17**, 499 (1964).

[26] J. Zhang, J. D. Zahn, W. Tan, and H. Lin, A transient solution for vesicle electrodeformation and relaxation, Phys. Fluids **25**, 071903 (2013).

[27] G. B. Arfken and H. J. Weber, *Mathematical Methods for Physicists*, 2nd ed. (Academic Press, 1970).

[28] H. Budiman and J. Talib, Prolate spheroidal coordinate: An approximation to modeling of ellipsoidal drops in rotating disk contractor column, J. Sci. Technol. **3**, 87 (2011).

[29] J. Bernhardt and H. Pauly, On the generation of potential differences across the membranes of ellipsoidal cells in an alternating electrical field, Biophysik **10**, 89 (1973).

[30] J. C. Lin, *Electromagnetic Fields in Biological Systems* (CRC Press, Boca Raton, FL, 2011).

[31] N. Bentenitis and S. Krause, Droplet deformation in dc electric fields: The extended leaky dielectric model, Langmuir **21**, 6194 (2005).

[32] E. Ley-Koo and G. Monsivais, Forces between two uniformly charged cylinders versus forces between two conducting cylinders, Rev. Mex. Fis. **45**, 108 (1999).

[33] P. Moon and D. E. Spencer, Separability in a class of coordinate systems, J. Franklin Inst. **254**, 227 (1952).

[34] P. Chaumet and J. Dufour, Electric potential and field between two different spheres, J. Electrost. **43**, 145 (1998).

[35] J. Raso, Fundamental and applied aspects of pulsed electric fields for microbial inactivation, in *1st World Congress on Electroporation and Pulsed Electric Fields in Biology, Medicine and Food & Environmental Technologies* (Springer, Berlin, 2016), pp. 11–14.

[36] A. Golberg and B. Rubinsky, The effect of electroporation type pulsed electric fields on DNA in aqueous solution, Technol. Cancer Res. Treat. **9**, 423 (2010).

[37] S. J. Beebe, P. Fox, L. Rec, K. Somers, R. H. Stark, and K. H. Schoenbach, Nanosecond pulsed electric field (nspef) effects on cells and tissues: Apoptosis induction and tumor growth inhibition, IEEE Trans. Plasma Sci. **30**, 286 (2002).

[38] P. M. Vlahovska, R. S. Gracia, S. Aranda-Espinoza, and R. Dimova, Electrohydrodynamic model of vesicle deformation in alternating electric fields, Biophys. J. **96**, 4789 (2009).

[39] Y. Sun, P. T. Vernier, M. Behrend, L. Marcu, and M. A. Gundersen, Electrode microchamber for noninvasive perturbation of mammalian cells with nanosecond pulsed electric fields, IEEE Trans. Nanobiosci. **4**, 277 (2005).

[40] E. Tekle, R. D. Astumian, and P. B. Chock, Electroporation by using bipolar oscillating electric field: An improved method for dna transfection of nih 3t3 cells, Proc. Natl. Acad. Sci. USA **88**, 4230 (1991).

[41] D. C. Sweeney, M. Reberšek, J. Dermol, L. Rems, D. Miklavčič, and R. V. Davalos, Quantification of cell membrane permeability induced by monopolar and high-frequency bipolar bursts of electrical pulses, Biochim. Biophys. Acta Biomembr. **1858**, 2689 (2016).

[42] T. Murovec, D. C. Sweeney, E. Latouche, R. V. Davalos, and C. Brosseau, Modeling of transmembrane potential in realistic multicellular structures before electroporation, Biophys. J. **111**, 2286 (2016).

[43] T. Kotnik, L. M. Mir, K. Flisar, M. Puc, and D. Miklavčič, Cell membrane electropermeabilization by symmetrical bipolar rectangular pulses: Part i. Increased efficiency of permeabilization, Bioelectrochem. **54**, 83 (2001).

[44] B. L. Ibey, J. C. Ullery, O. N. Pakhomova, C. C. Roth, I. Semenov, H. T. Beier, M. Tarango, S. Xiao, K. H. Schoenbach, and A. G. Pakhomov, Bipolar nanosecond electric pulses are less efficient at electropermeabilization and killing cells than monopolar pulses, Biochem. Biophys. Res. Commun. **443**, 568 (2014).

[45] A. G. Pakhomov, I. Semenov, S. Xiao, O. N. Pakhomova, B. Gregory, K. H. Schoenbach, J. C. Ullery, H. T. Beier, S. R. Rajulapati, and B. L. Ibey, Cancellation of cellular responses to nanoelectroporation by reversing the stimulus polarity, Cellular and molecular life sciences **71**, 4431 (2014).

[46] See Supplemental Material at http://link.aps.org/supplemental/10.1103/PhysRevE.101.062407 for comparison between FEM simulation and analytical treatment for ac and dc fields.

[47] W. Frey, J. White, R. Price, P. Blackmore, R. Joshi, R. Nuccitelli, S. Beebe, K. Schoenbach, and J. Kolb, Plasma membrane voltage changes during nanosecond pulsed electric field exposure, Biophys. J. **90**, 3608 (2006).

[48] T. Y. Tsong, Electroporation of cell membranes, in *Electroporation and Electrofusion in Cell Biology* (Springer, Berlin, 1989), pp. 149–163.

[49] H. B. Kim, S. Lee, J. H. Chung, S. N. Kim, C. K. Sung, and K. Y. Baik, Effects of actin cytoskeleton disruption on electroporation in vitro, Appl. Biochem. Biotechnol. (2020), doi: 10.1007/s12010-020-03271-4.

[50] D. Xiao, L. Tang, C. Zeng, J. Wang, X. Luo, C. Yao, and C. Sun, Effect of actin cytoskeleton disruption on electric pulse-induced apoptosis and electroporation in tumour cells, Cell Biol. Int. **35**, 99 (2011).

[51] W. Krassowska and P. D. Filev, Modeling electroporation in a single cell, Biophys. J. **92**, 404 (2007).